



The Messinian Ebro River incision

R. Pellen^{a,*}, D. Aslanian^b, M. Rabineau^a, J.P. Suc^c, C. Gorini^c, E. Leroux^b, C. Blanpied^c, C. Silenziario^d, S.M. Popescu^e, J.L. Rubino^f



^a CNRS, Université de Bretagne Occidentale, Univ. Bretagne Sud, UMR6538 Laboratoire Géosciences Océan, IUEM, 1 place Nicolas Copernic, 29280 Plouzané, France

^b IFREMER, Laboratoire Géodynamique et enregistrements Sédimentaires, BP70, 29280 Plouzané, France

^c Sorbonne Universités, UPMC University Paris 06, CNRS, Institut des Sciences de la Terre de Paris (iSTEPI), UMR 7193, 4 place Jussieu, 75005 Paris, France

^d Schlumberger Italiana SPA, Via dell'Unione Europea, 4 – Torre Beta, 20097 San Donato Milanese, Italy

^e GeoBioStratData.Consulting, 385 route du Mas Rillier, 69140 Rillieux la Pape, France

^f TOTAL, TG/ISS, CSTTF, Avenue Laribea, 64018 Pau Cedex, France

ARTICLE INFO

Keywords:

NW Mediterranean Sea
Segmentation
Knickpoint
Ebro fluvial system
Messinian Salinity Crisis
Incised-valley system

ABSTRACT

Morphological sills condition sedimentary, water and fauna exchanges between different domains. In particular, sills are crucial factors to consider during the Messinian Salinity Crisis (MSC) palaeogeographic evolution (5.97–5.33 Ma) of the NW Mediterranean area. Here we focus on the Ebro River and its up to now unexplained short Messinian onshore length (~100 km) compared to that of the Messinian Rhone River (~480 km) despite similar present-day drainage basins. Thanks to an extensive seismic and borehole dataset, we present a new interpretation of a complete 270 km long Messinian Ebro incised-valley system course underneath the present-day continental margin and bathyal basin and its related distal detrital deposits. These results favour a syn-MSC or pre-MSC opening of the (endorheic) Ebro Basin to the Mediterranean. We propose a mechanism of retrogressive erosional process, localized at structural knickpoints that shift seaward through time. This mechanism resulted in the development of the complete incised-valley system and the falling stage system tract (FSST) during the MSC sea level fall with negligible or even null retrogressive inland erosion beyond the Catalan Coastal Range. The shifting of erosion-deposition is controlled by the pre-Messinian stepwise morphology and segmentation in the Valencia, Menorca and Liguro-Provence Basins. By comparison, the Rhone system is simpler, characterized by the key role of a single knickpoint (at the shelf-break) and a steeper continental slope. Both cases highlight the relationship between kinematic, segmentation and their relative morphologies, base-level fall and erosional/depositional response particularly well expressed during the outstanding MSC associated with a huge relative sea-level drop that we measured down to -1100 m below present day sea-level.

Abbreviations

General	Stratigraphy
ESP Expended Spread Profile	FAD First Appearance Datum
Km Messinian Knickpoint	FSST Falling Stage System Tract
Ka Present-day knickpoint	HST Highstand System Tract
MSC Messinian Salinity Crisis	LAD Last Appearance Datum
Twt Two-Way Travel time	LST Lowstand System Tract
Geography	LU Lower Unit
CCR Catalan Coastal Range	MES Messinian Erosional Surface
CFZ Central Fracture Zone	MRS Maximum Regression Surface
EB Ebro Basin	MLM Messinian Lower Megasequence
GOL Golf of Lion	MUM Messinian Upper Megasequence
LPB Liguro-Provence Basin	MU Mobile Unit
MB Menorca Basin	RSME Regressive Surface of Marine Erosion
NBFZ North Balearic Fracture Zone	TST Transgressive System Tract
VB Valencia Basin	UU Upper Unit

1. Introduction

Morphological sills, whether related to sedimentary, inherited structural reliefs or originating from the kinematic history, play a crucial role in the sedimentary, water and fauna exchanges between basins through time. These sills often fit areas of different crustal nature and different subsidence histories, as observed in the Mediterranean-Paratethys area (e.g. Leever et al., 2010; Leroux et al., 2015a; Palcu et al., 2017; Pellen et al., 2017). In the case of huge relative sea-level variations, as during the MSC (5.97–5.33 Ma) (Manzi et al., 2013), consideration of these barriers is of primary importance to understand the morphological and sedimentary evolution of the different basins (e.g. Leever et al., 2010; Flecker et al., 2015; Palcu et al., 2017; Suc et al., 2015; Balázs et al., 2017).

* Corresponding author.

E-mail address: romain.pellen@univ-brest.fr (R. Pellen).

1.1. The Ebro Paradox

The Rhone and Ebro fluvial systems are excellent examples of major rivers in the Mediterranean Sea (the 2nd and 3rd respectively after the

Nile) that experienced the same crisis in response to the isolation of the Mediterranean Sea. Present-day drainage areas are of similar size (nearly 99,000 km² and 86,000 km², respectively) (Babault et al., 2006) (Fig. 1). However direct comparisons between the Messinian palaeo-

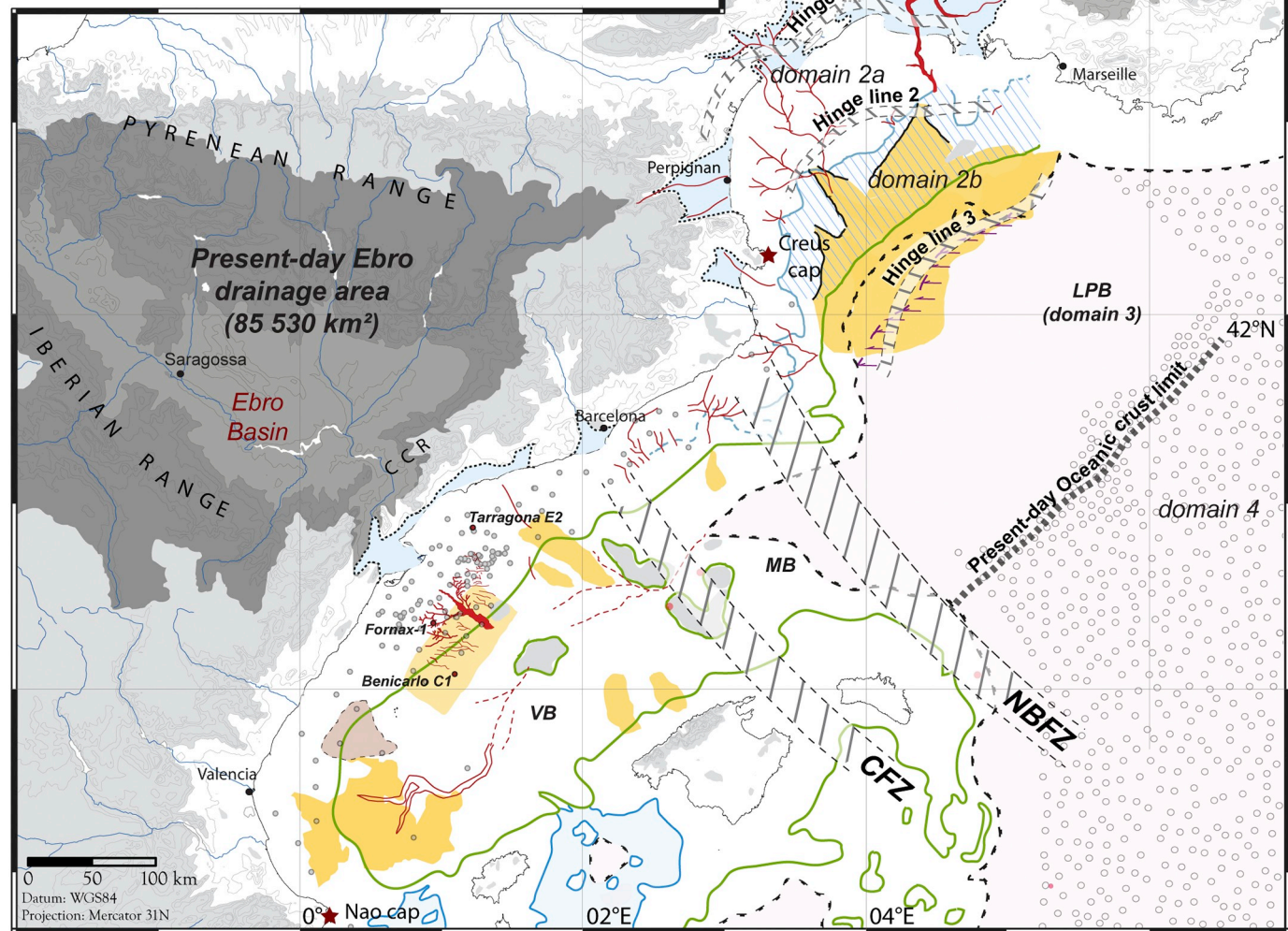
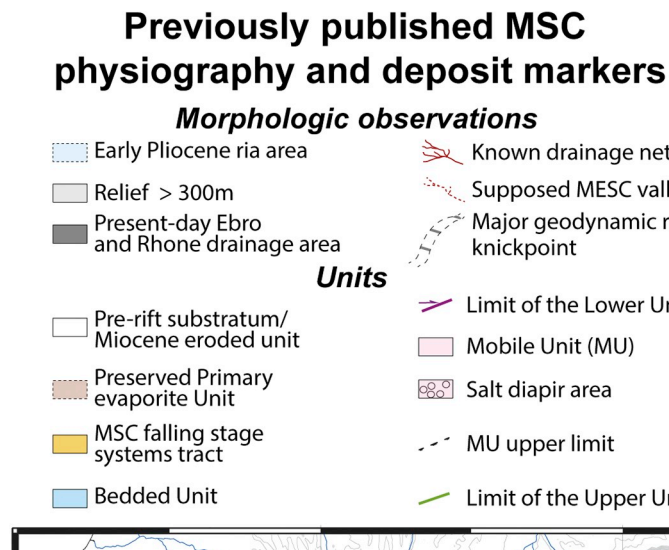


Fig. 1. A Present-day NW Mediterranean physiographic areas and previously published major physiographic features and seismic units assigned to the Messinian event (compiled from Stampfli and Hoëcker, 1989; Frey-Martinez et al., 2004; Maillard and Mauffret, 2006, Maillard et al., 2006; Del Olmo, 2011; Garcia et al., 2011; Urgeles et al., 2011; Bache et al., 2009, Bache et al., 2015). Major geodynamic boundaries are represented in the Valencia-Menorca Basin (VB-MB): C.F.Z. = Central Fracture Zone; N.B.F.Z. = North Balearic Fracture Zone (Maillard and Mauffret, 1999; Pellen et al., 2016) and in the Liguro-Provence Basin (LPB): domain 1 = Unthinned Continental Crust; domain 2a = Thinned Continental Crust; domain 2b = Highly thinned Continental Crust; domain 3 = Exhumed lower crust; domain 4 = Atypical oceanic crust (Moulin et al., 2015; Leroux et al., 2015a, 2015b).

Mapping the MSC physiography and deposit markers (VB & LPB domains)

Morphologic observations

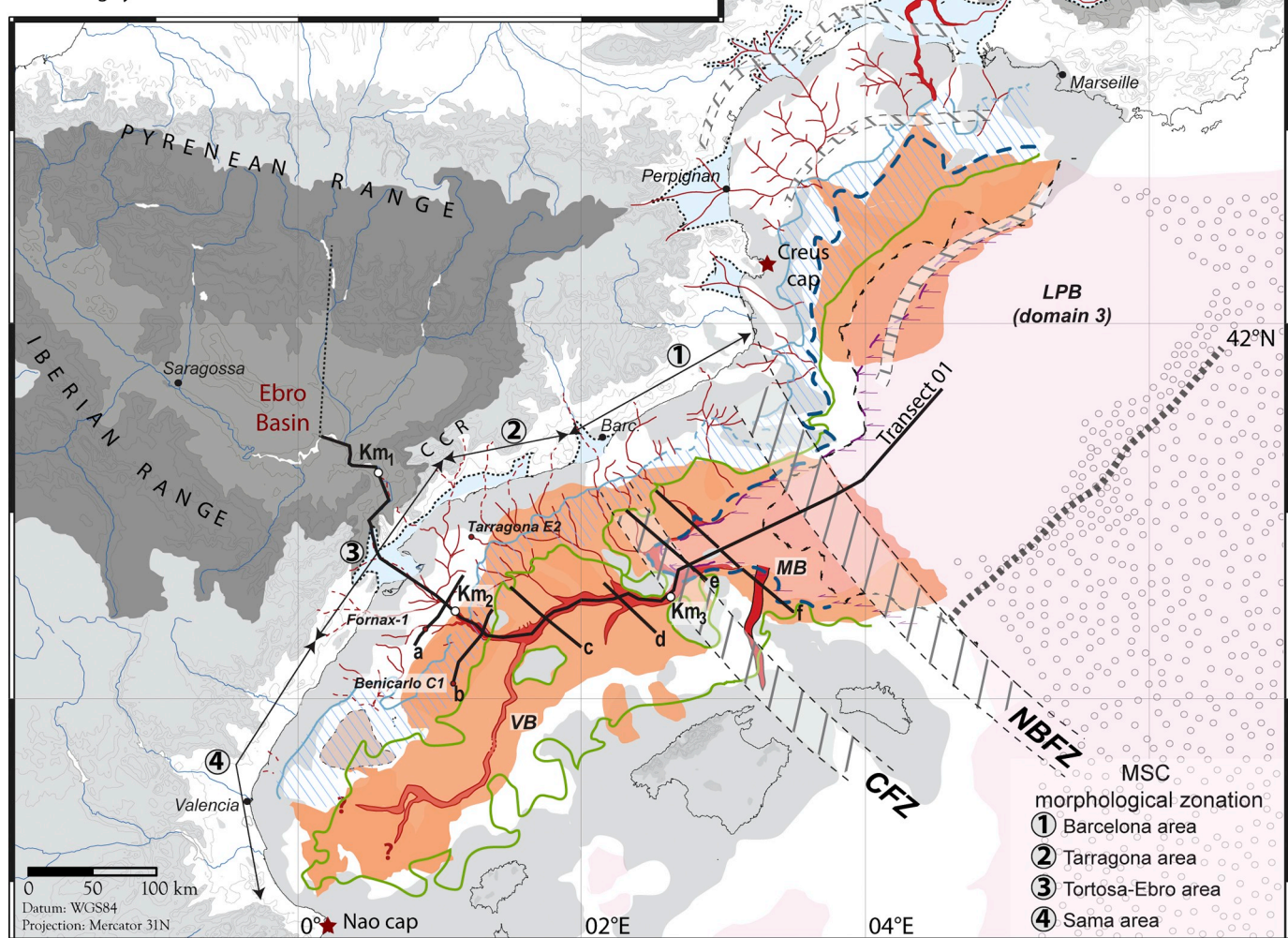
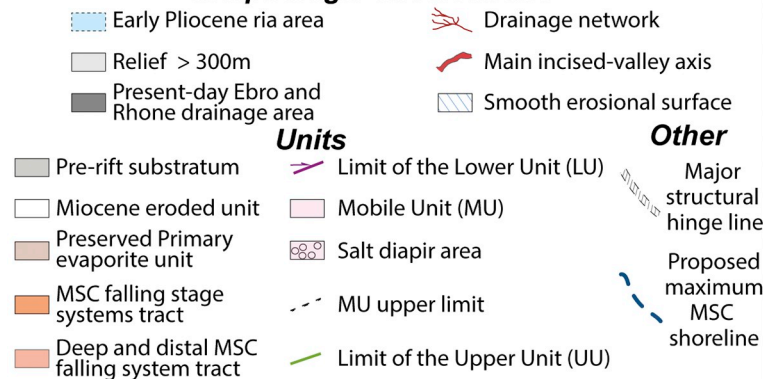


Fig. 2. Map showing our new interpretation of the sedimentary units and main morphological observations associated to the Messinian event in the VB-VM. The Messinian drainage network (in red) could be followed from the shelf to the VB and up to the MB. Position of vertical sections a to f shown in black (see Fig. 3). (For interpretation of the references to colour in this figure legend, the reader is referred to the web version of this article.)

Ebro and Messinian palaeo-Rhone systems point out the so-called “Ebro paradox” (Babault et al., 2006): despite similar present-day drainage areas, the length of the Messinian subaerial incision of the Ebro river seems much shorter than that of the Rhone river. In the case of the Messinian palaeo-Rhone, a total 480 km long fluvial incision network was described along the Alps (Clauzon, 1982, 1999) to the pre-Messinian Platform edge (Bache, 2008) (Fig. 1). In the case of the Messinian

palaeo-Ebro erosion system, the incision is limited to about 100 km from the Catalan Coastal Range (CCR) edges to the former pre-Messinian platform edge (Fig. 1) (Urgeles et al., 2011) with no major incision described in the endorheic Ebro Basin. Why such a difference? Babault et al. (2006) proposed that the Ebro River did not exist before the Messinian Salinity Crisis and that the connection between the endorheic Ebro Basin to the Mediterranean Sea occurred after the MSC (or

potentially during this phase).

Conversely, several authors consider that seismic data provide evidence of well-developed sedimentation and deltaic progradation during the Tortonian and the development of a main incised-valley system during the MSC, implying a Tortonian connection between the Ebro Basin (EB) and the Valencia Basin (VB) (e.g. Arche et al., 2010; Cameselle et al., 2014). Recent modeling and field data on the foreland EB further argued that the transition from endorheic to exorheic of Ebro is pre-Messinian, although the precise timing remains to be established (12 to 7.5 Ma) (Fillon et al., 2013; Garcia-Castellanos and Larrasoña, 2015). However, the absence of major fluvial incision towards the onshore EB, the short incision of ~100 km and the absence of well-described detrital *syn*-MSC deposits in the VB remain unanswered. Indeed, Messinian clastic deposits were only partially described and mainly on the (present-day) outer shelf. These deposits were described either on top (Escutia and Maldonado, 1992; Maillard and Mauffret, 2006, Maillard et al., 2006, or below the so-called Upper Unit (UU, Garcia et al., 2011; Cameselle et al., 2014, Garcia-Castellanos and Larrasoña, 2015) of the well-known Messinian trilogy (LU-MU-UU) synthesised by Lofi et al. (2011) (Fig. 1). This peculiar morphology strongly contrasts with that of the Western, Gulf of Lion, and Eastern, Nile region, Mediterranean that both show long fluvial system incisions and large detrital deposits during the Messinian sea-level fall (Gorini et al., 2015) and remain to be explained.

1.2. Geodynamic and stratigraphic framework

The Neogene palaeoenvironmental framework of the NW Mediterranean region is largely conditioned by geodynamic history which controls the vertical motion and sedimentation in each sub-basin (Leroux et al., 2015a, 2015b; Pellen et al., 2016). The geometry and physical link between the evaporitic and detritic successions, and major tectonic hinge lines are well known in the Liguro-Provence Basin (LPB, Bache et al., 2015; Leroux et al., 2015a) (Fig. 1). However, a complete regional stratigraphic and morphological seismic study linking the CCR edges to the deep LPB is still lacking.

A NW-SE segmentation distinguishes the MB from the Mesozoic VB (Roca and Guimerà, 1992; Etheve et al., 2016, 2018) and the deep LPB (Fig. 1): the Central and North Balearic Fracture Zones (CFZ and NBFZ) represent two major sills that created a stepwise accommodation between the three domains (Pellen et al., 2016). The geodynamic process leading to the formation of these sills is rooted in the counter-clockwise rotation of Corsica-Sardinia block during the early Miocene which drove the movement of Menorca Island, and non-kinematic motion of Ibiza-Majorca islands (Pellen et al., 2016). These motions distinguish early Miocene LPB and MB basins from the Mesozoic VB basin (e.g. Olivet, 1996; Gueguen et al., 1998; Bache et al., 2010; Pellen et al., 2016; Etheve et al., 2016). One of the main consequences is a different subsidence history for each basin, with purely vertical Neogene “sag” subsidence for the Mesozoic VB (Pellen et al., 2016).

A NW-SE segmentation shapes the GOL-LPB with five differentiated crustal domains on the French side (Moulin et al., 2015; Afilhado et al., 2015; Jolivet et al., 2015): unthinned continental crust, thinned continental crust, highly thinned continental crust, exhumed lower continental crust and proto-oceanic crust. Three domains of subsidence were found defined by three hinge lines (Figs. 1, 2). On the platform and slope, the subsidence takes the form of a seaward tilt with different amplitudes, whereas the deep basin (with exhumed lower continental crust and proto-oceanic crust) subsides purely vertically (Leroux et al., 2015a, 2015b).

The shelves of the MB and the GOL (domain 2a) (Fig. 1) first record a late Oligocene-Aquitian marine influx (Roca and Guimerà, 1992; Bartrina et al., 1992; Roca, 2001; Bache et al., 2010), followed by Burdigalian-Tortonian clay-marl then sand deposits associated with a prograding trend. The outermost position of this Tortonian shelf is shown on Fig. 1 (from Bache, 2008). The deep part of the LPB and MB

are usually associated with condensed Burdigalian-Tortonian deposits (Roca, 2001). The Mesozoic VB (Roca and Guimerà, 1992; Etheve et al., 2016, 2018) experienced the first marine ingressions during the late Burdigalian-Langhian followed by an enhanced Tortonian prograding trend in the Tortosa area (Clavell and Berastegui, 1991; Cameselle et al., 2014; Pellen et al., 2016).

1.3. Ebro versus Rhone inheritances

The initiation of the endorheic sedimentation in the EB has been estimated at ~35 Ma (Costa et al., 2010), the final preserved lacustrine fill stage is proposed to be at least 13.5 and 12 Ma (in Urgeles et al., 2011) and up to Tortonian (e.g. Vasquez-Urbez et al., 2013). At the time of the basin's opening towards the Mediterranean Sea, an elevation of 535–750 m above sea level has been estimated (Garcia-Castellanos and Larrasoña, 2015) which places the Catalan Coastal Range (CCR) as an important morphological barrier between the VB and EB. At the dawn of the MSC, a stepped morphology is observed for the VB-MB where offshore knickpoints are located at the edge of the Miocene platform or at major geodynamic boundaries (Fig. 2). On the contrary, the GOL is characterized by a single continental slope (Guennoc et al., 2000). Furthermore, no major geodynamical sill is observed along the onshore Rhone drainage system (Séranne, 1999; Guennoc et al., 2000; Sissingh, 2001).

In this study, based on a large set of seismic and borehole data, we made a detailed synthesis of the offshore physiography during Messinian, by correlating the VB, MB, and LPB with seismic stratigraphic and geomorphological methods tied to existing borehole data with revisited detailed biostratigraphic analysis to propose a new understanding of Ebro and Rhone systems evolution during the MSC.

2. Data and method

2.1. Dataset

Our study is based on a large set of seismic and borehole data collected during the extensive French academia-industry programs (Actions-Marges, GRI Tethys Sud), in close collaboration with the Total and Schlumberger groups as well as data available from the Spanish SIGEOF database. This compilation provided for the correlation of seismic markers from the VB towards the LPB (as shown already in Pellen et al., 2016). Twenty-four petroleum wells drilled between 1969 and 2004 along the NE Iberian margin have been used to calibrate seismic interpretations, although the stratigraphic information was often sparse or vague. We used the detailed stratigraphic, sedimentological and micropaleontological information available from three wells located on the present-day Ebro platform to constrain ages and palaeoenvironments of identified surfaces and units: Fornax 1 (Bailey et al., 2008; Urgeles et al., 2011; Cameselle et al., 2014; Mauffrey et al., 2017), Benicarlo C1 (this study) and Tarragona E2 (Evans et al., 1978; Bessais and Cravatte, 1988).

In this paper the detailed lithological, environmental and biostratigraphic information from the Benicarlo C1 are provided for Miocene-Messinian-Pliocene series (based on Evans et al., 1978) that we have revisited in the light of recent biostratigraphic charts, a modern geological time scale (Gradstein et al., 2012) and correlation with more regional information (see chapters 3.2 to 4.2).

2.2. Sequence stratigraphy

Conventional seismic stratigraphic method was used (Mitchum and Vail, 1977; Vail et al., 1977) to identify seismic discontinuities and stratigraphic surfaces and units based on reflexion configurations and facies characteristics (See the Table in Supplementary Material 3 for details of surfaces and units). However, identified surfaces and units were interpreted using principles of sequence stratigraphy in their

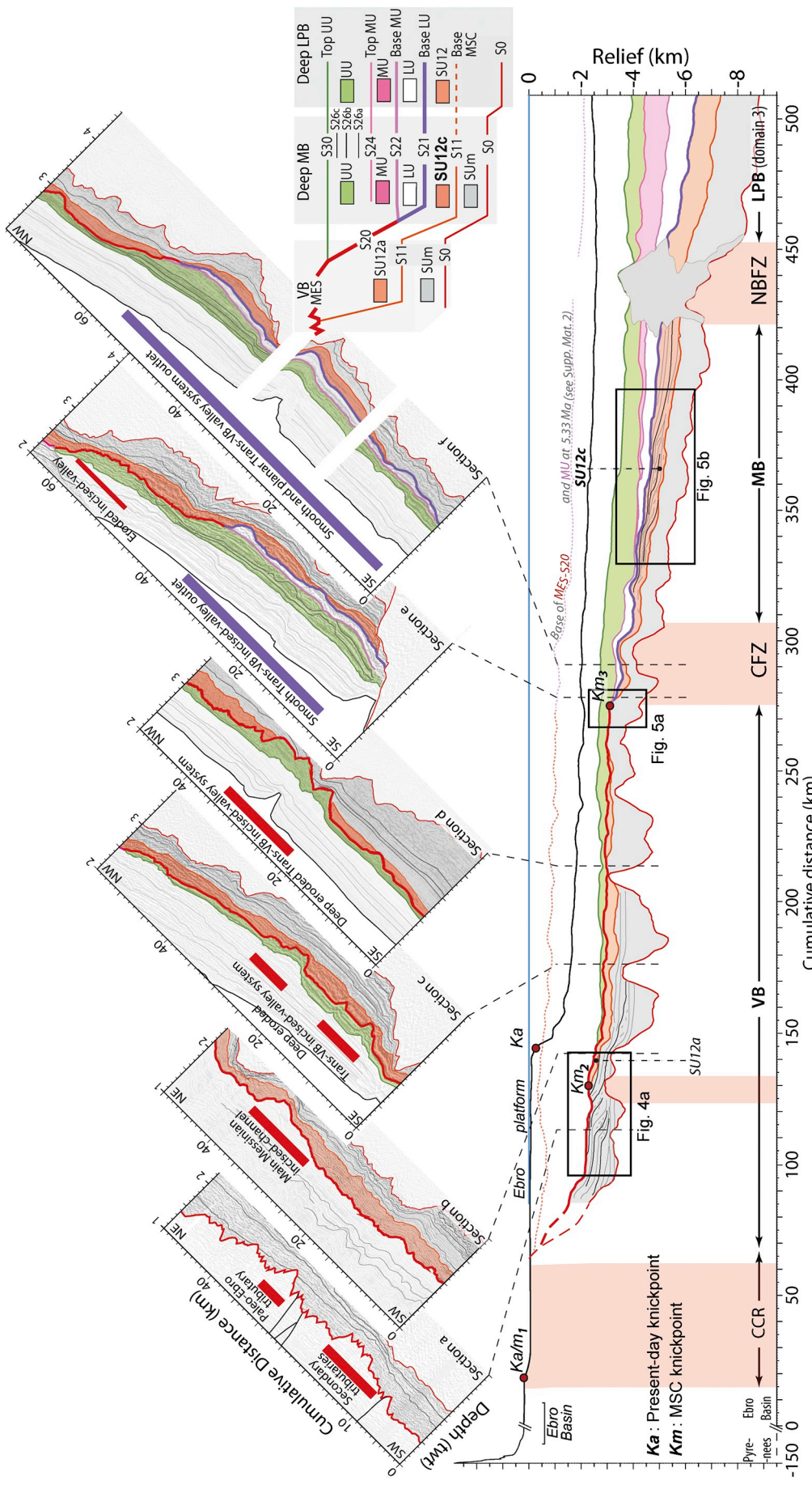


Fig. 3. Seismic sections a-f showing the morphological evolution of the trans-VB Messinian valley system, its outlet and the related Messinian detrital and evaporitic deposits. The red marker symbolizes MES and S20 rough surface, the violet markers symbolize the smoother S21 surface at the outlet of the valley system. Transect01 is a composite dip section converted in depth (see methods and supplementary figures for more details) from the VB to the deep LPB. Note in particular the progressive downward shifts of top of units 12a and 12c. Dotted lines along Transect01 represent the position of MES-S20 and S22 at the end of the MSC (5.33Ma). Position of the profiles is given in Fig. 2. (For interpretation of the references to colour in this figure legend, the reader is referred to the web version of this article.)

revised most recent version i.e. including interpretation of Falling Stage System Tract (FSST) (e.g. Hunt and Tucker, 1992; Catuneanu et al., 2011), forced regression concept (e.g. Plint, 1988) with Maximum Regression surface (MRS) and Regressive Surface of Marine erosion (RSME) (e.g. Helland-Hansen and Hampson, 2009). Ages of these sequences were provided by well data. Our interpretations were then integrated into the 'Kingdom Suite' software to insure coherency at all crossing lines. For the Messinian units, we used the now well established so-called « Messinian-trilogy » Lower Unit (LU)/Mobile Unit (MU)/ Upper Unit (UU) as synthesized by Lofi et al. (2011). Nevertheless, we provide special focus on units and sub-units related to clastic units (see results below).

2.3. Time to depth conversion and backstripping

Our seismic interpretations were converted from time to depth using average sediments velocities (layer cake model), to obtain the geometries in depths (meters) of surfaces and sedimentary units (Fig. 3, Transect01). Seismic velocities strongly vary in space within the same stratigraphic interval, with significant variations between the shelf, the base of slope, and the basin. Compiled borehole velocities on the VB platform and on the foot slope, as well as ESP velocities located in the deep LPB (Leroux et al., 2017) were used to estimate an average velocity for each layer (see velocity model in Supplementary material 1). The depth converted profile allowed us to measure the difference in altitudes between key points along the profiles, and sedimentary unit thicknesses.

A simple 2-D backstripping was performed to reconstruct geometries through time (in particular at early Zanclean, at Messinian low stand incised-system and related deposits (see details in Supplementary material 2). Input parameters for the VB domain include paleobathymetry, age, and porosity of sedimentary packages based on Urgeles et al. (2011). An estimated total subsidence value up to 960 m/Ma for the deep LPB domain was also applied to the 2-D backstripping for Pliocene-Quaternary times as quantified by Rabineau et al. (2014).

2.4. Knickpoint definition and chosen approach

Our study used the identification of knickpoints, highlighted either by morphological change or new sedimentary sequences development along the seismic profile. Different processes are associated with onshore and offshore development of such morphological features. On land, knickpoints are interpreted as resulting from renewed erosion of a rejuvenated river that propagates upstream and influences the development of landscapes and source-to-sink systems (Grimaud et al., 2016). They are usually triggered by a relative fall in river base-level (either through eustatic sea-level drop, tectonic faulting or uplift) and can also highlight the onshore-offshore position (Goswani et al., 2017). Submarine knickpoints are often located at the shelf-break creating an offlap-break either (i) at the transition between the outer shelf and the continental slope (e.g. Rabineau et al., 2014), or (ii) at the boundary of domains where tectonic motion displaces the seafloor (Amblas et al., 2011) or (iii) at the site where channel levees are breached. Knickpoints are key elements to take into account in when considering segmented domains, we therefore paid a particular attention to their identification.

Below, we present our results from the onshore domain towards the deeper offshore domains.

3. Results

3.1. Morphology from seismic interpretation

Fig. 3 presents our stratigraphic interpretation across the VB-MB along six seismic profiles perpendicular to the main erosional incision. Transect 01 has been converted to depth. Eight major seismic surfaces

are illustrated, S0 (Tertiary basement), MES, S11, S20, S21, S22, S24, and S30 which respectively delimit four seismic units: SU12a-c, LU, MU and UU and three major knickpoints (Km1–3). Three secondary surfaces (S26a, b, c) are also identified in the UU. Relationships, age and interpretations of surfaces and units are presented in the table in Supplementary material 3.

The first knickpoint Km₁ is located at the transition between the former foreland EB (~535 m above sea level) and the VB at the edges of the CCR (Figs. 2 and 3). Below this knickpoint, the Marginal Erosional Surface (MES, Lofi et al., 2011) shows a highly rugged and dissected surface with frequent incisions organized in a dendritic pattern (also interpreted on 3D seismic data, e.g. Urgeles et al., 2011, and Cameselle et al., 2014) (Figs. 2 and 3, section a). Four palaeo-drainage systems are observed (Fig. 2) that present numerous incised fluvial tributaries with rough badland-like morphology of the MES (Urgeles et al., 2011) above the isocontour of 1.6 s TWT (~2.5 km depth) below present-day sea level. It is worth noting that the MES truncates the former Tortonian prograding clinoforms which form the Miocene platform in the Tortosa-Ebro domain (Figs. 3 and 4). This is also confirmed by the Tarragona E2 well which sampled Tortonian deposits just below the MES (Bessais and Cravatte, 1988). A wide dendritic palaeo-drainage system is mapped for the Tortosa-Ebro domain (Fig. 2) which is the main and deepest NW-SE river channel interpreted as the Messinian Ebro fluvial system (Urgeles et al., 2011) (Figs. 2, 3 section a & b). A ~61 km long main channel incision can be measured from the pre-MSC coast to the Tortosa-Ebro lower slope.

The erosive surface S11 extends seaward of the MES at the position of the Km₂ (Fig. 3, Transect01 - km 130; Fig. 4) at the Miocene platform edge, delimiting the base of SU12a showing downlapping prograding clinoforms geometries. Only the bottomset part of the clinoforms has been preserved on both sides of the main Messinian river channel. The basal erosive surface S11 also marks a change in the progradational trend along the Miocene platform edge (Fig. 4, section h) of the Tarragona area: A major change in direction of sediment input from the morphological domain of Barcelona to the Tortosa-Ebro domain is highlighted by the basal erosive surface S11.

S11 shows a generally smoother morphology towards the VB foot-slope domain. In this area the MES subtracts into two erosive surface: the basal erosive surface S20 which truncate the seismic unit SU12a while the top erosive surface S30 bound the UU seismic unit (Fig. 3, sections c, d). Along the former Miocene outer shelf, the MES-S20 surface shows a smoother erosive surface below 2.5 km depth (Fig. 4, sections g, h) with the disappearance of badland morphology except in the axis of the main channel incision (Fig. 3, section b; Fig. 4). The extension of the S20 surface across the VB foot-slope domain highlights the lateral continuation of an incised channel along the VB domain. A slight NE-ward inclination is observed along the incised-valley profile with a mean present-day depth position ranging from 2.8 km below sea level at the Tortosa domain foot-slope to 3.2 km depth at its outlet (Fig. 3, sections c-f). The morphology shows an evolution from a ~6 km wide with an interfluvial/thalweg height of 370–400 m at the toe of the proto-Ebro slope offshore the Tortosa-Tarragona domain (Fig. 3, sections a-c) to a ~16 km wide, 100–130 m deep incision at the transition towards the MB (Fig. 3, sections d, e). Bedrock morphology partly deflects the path of the incised-valley and slightly influences its sinuosity (Figs. 2, 3, section c).

On both sides of this SW-NE valley, which totals a length of ~134 km in the deep VB domain, the surface is relatively conform compared to the underlying deposits. The main incised-valley is joined by two smaller tributaries from the SW part of the VB and already mapped by Cameselle and Urgeles (2015).

At the transition between the VB and MB (CFZ area in Figs. 2, 3 and 5, section i) (Maillard and Mauffret, 1999; Pellen et al., 2016), S20 shows another knickpoint Km₃ (~3.2 km depth, at Transect01, km 270 in Fig. 3). It marks: 1) the deepening of the basal surface S11 and its overlying unit SU12c – as the lateral correlation of SU12a; 2) the last

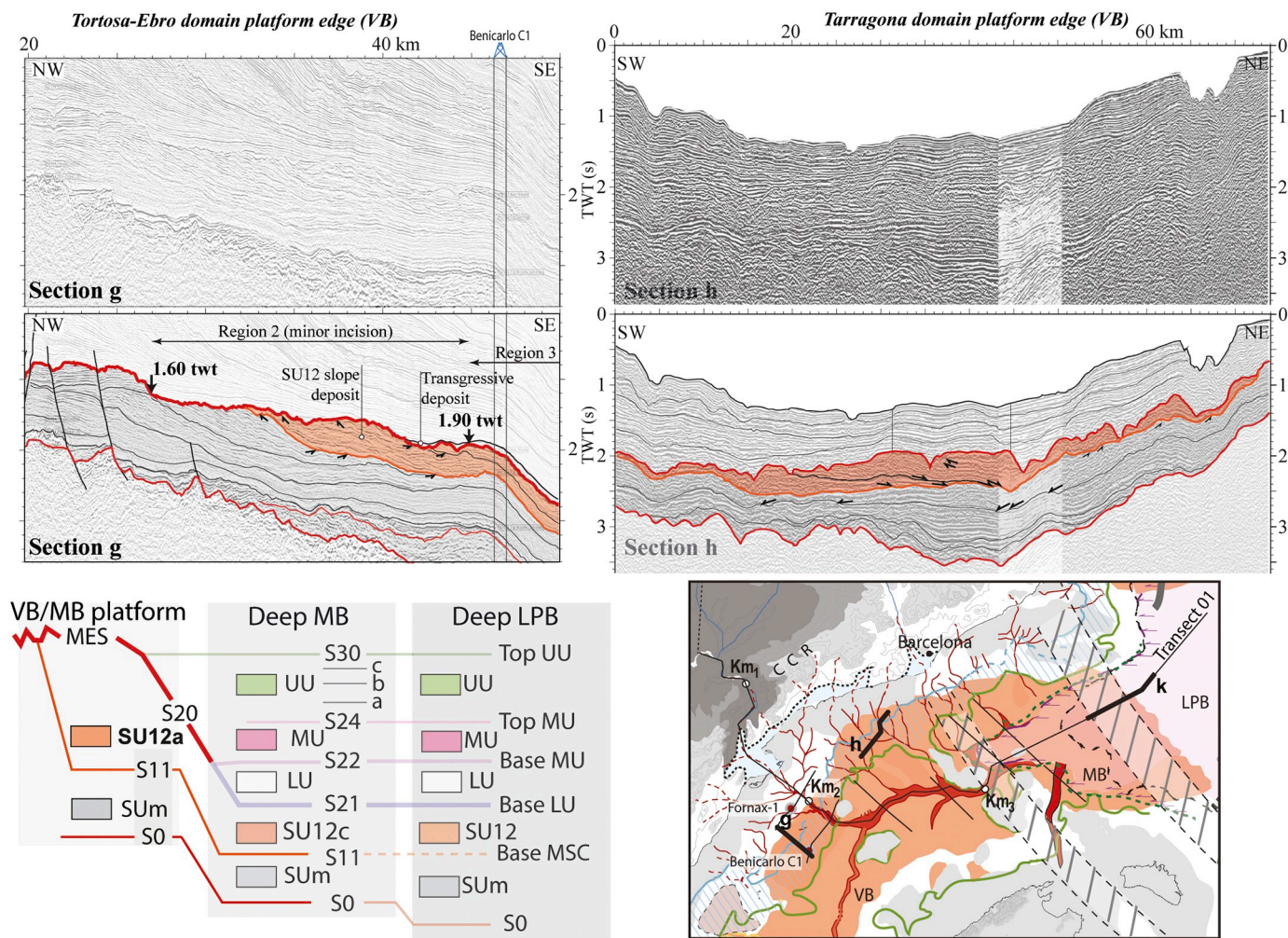


Fig. 4. Detailed seismic section highlighting the development of a Miocene ante-MSC platform along the Ebro-Tortosa area (section g) which mark Km2 knickpoint. The development of SU12a is associated to a regressive surface of marine erosion (RSME) (section g) and to a major change in the origin of sediment supply (section h).

S20 toplap features; 3) the formation of two new surfaces, S21 – as the lateral correlation of S20 – and S22 at the top and 4) the thickening of the UU.

The S12 and S21 surfaces delimitates the development of SU12c with the NE-ward preserved prograding clinoforms (Fig. 5, section j). S21 at the top of SU12c also shows some widespread erosion and becomes smoother and conformable towards the MB-LPB transition (Fig. 3, section f). The conformable and non-incised S21 development also highlights the formation of the overlying LU. Both observations attest the termination of the trans-VB incised-system thus marking its outlet at the VB-MB transition.

The continuity of the erosional system from the VB platform to the Km₃ knickpoint therefore points to a 270 km long system that we identify as the trans-VB Messinian valley system (Figs. 2 and 3, Transect 01 and sections b-d). The MB-LPB transition marked by the North Balearic Fracture Zone (NBFZ) corresponds to the full development of the Messinian trilogy units (LU-MU-UU) as identified in the deep LPB domain (Figs. 3 and 9).

Using the backstripped section of Transect01 at 5.3 Ma (i.e. at the end of the MSC), we measure the general slope of the MES-S20-S21 from 90 to 430 km as equal to 0.55% (i.e. 0.32°). However, individual segments in between knickpoints show a slope even smaller than 0.4% (0.23°) and 0.45% (0.26°), between 90 and 280 km and 310–430 km respectively. Conversely, surface S11 at the base of SU12c shows a slope of 1.58% (0.9°), between 310 and 430 km.

3.2. Borehole data

3.2.1. Biostratigraphy

The Benicarlo C1 well (Fig. 6) provided planktonic foraminifers recorded from cuttings (Evans et al., 1978). These data have been revisited and evaluated in light of the most recent biostratigraphic zonation in the Mediterranean (Iaccarino et al., 2007) and the modern geological time scale (Gradstein et al., 2012).

The top of Cretaceous limestones (Upper-Middle Cenomanian) is well identified at 4330 m depth. With respect to several Mediterranean long records (Suc et al., 1992; Lirer and Iaccarino, 2011), the base of Pleistocene deposits (i.e. the base of the Gelasian, at 2.6 Ma) can be assessed between 2330 m depth (uppermost occurrence of *Sphaeroidinellopsis subdehisca*, usually estimated at 3.2 Ma) and 2060 m (lowermost occurrence of *Globorotalia inflata*, dated at 2.09 Ma in the Mediterranean Sea; Iaccarino et al., 2007). Consequently, our biostratigraphic re-evaluation focuses on the depth interval 4300–2300 m, which encompasses the Middle-Late Miocene and whole Pliocene (Fig. 6). Examining the vertical distribution of the species with a biostratigraphic significance along the studied interval, we paid particular attention to discontinuous occurrences, some punctual records may result from cavings or reworkings.

Orbulina universa is present from 4240 m depth that suggests an age younger than 14.10 Ma (First Appearance Datum, FAD, of the species in the Mediterranean; Iaccarino et al., 2007). *Neogloboquadra acostaensis*

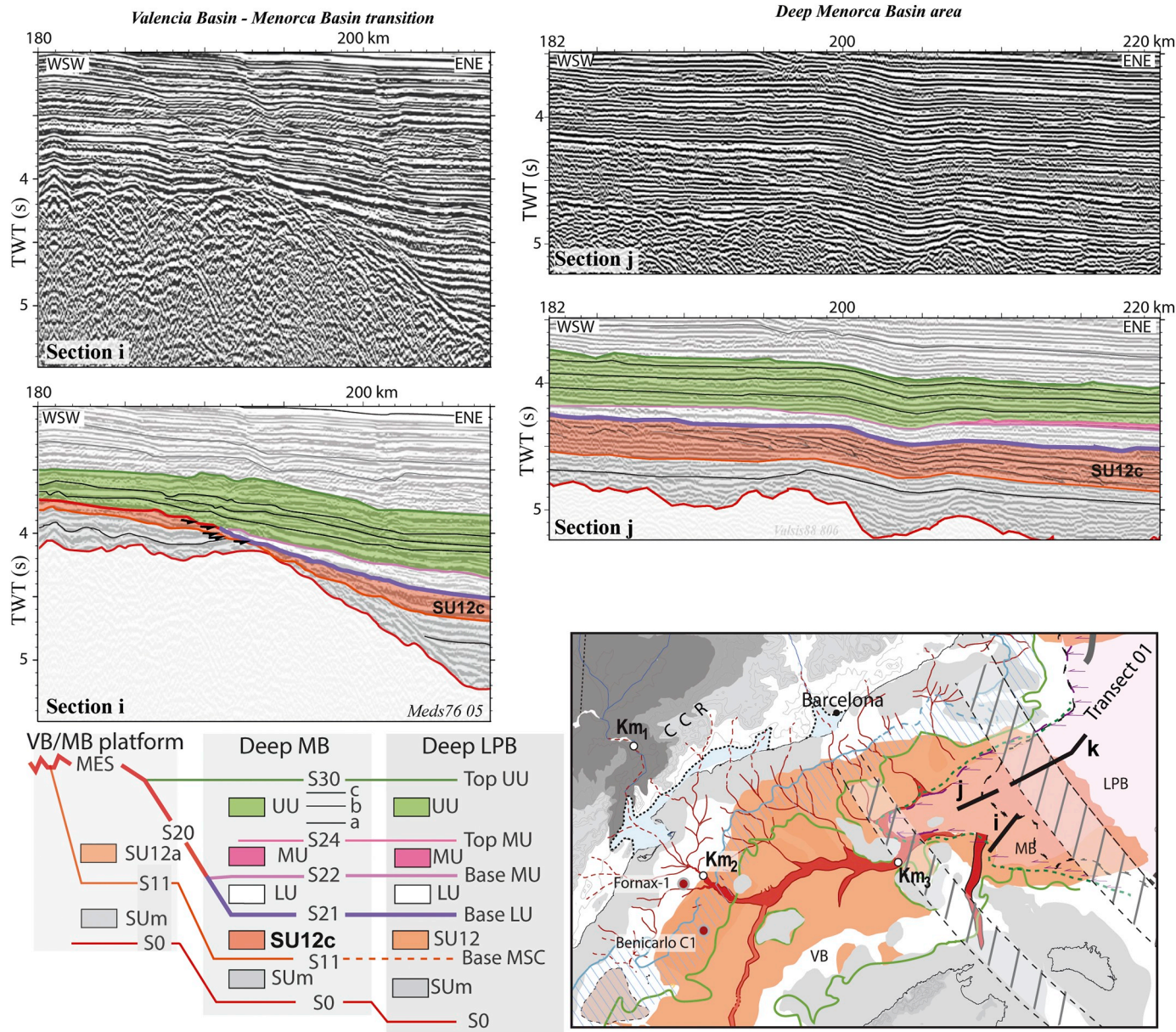


Fig. 5. Detailed seismic section highlighting the erosional truncations at the transition between the VB and the MB domain (section i) and development of the progradational seismic units SU12c in the deep and distal MB area (section j). We interpret this SU12c unit as the LST related to the MSC, it corresponds to the most distal progradating detritic unit observed in the area.

has been continuously recorded from 4240 to 4180 m, then intermittently at 3830 m, and continuously from 3710 m to 2040 m. The FAD of *N. acostaensis* in the Mediterranean Sea is dated at 11.90 Ma. Two interpretations can be discussed: (1) to place the FAD of *N. acostaensis* at 4240 m or (2) to place it at 3710 m. Hypothesis 1 implies very thick deposits to be ascribed to Tortonian while hypothesis 2 suggests that deposits from the base of the studied interval partly belong to the Serravallian and maybe to the Langhian. Caliper log (Fig. 6) suggests the presence of numerous caving effect between 3600 m and 4240 m which would affect the record of *N. acostaensis* or *Orbulina universa* below 3710 m. As well, the biostratigraphic interpretation of the nearby Tarragona E2 well (Cravatte, 1980; Bessais, 1984; Bessais and Cravatte, 1988) would be more consistent with the second hypothesis. Accordingly, sediments between 4240 and 3710 m depth could belong to a time-interval running from biozone MMi5 to biozone MMi10 (Fig. 6).

Above, the continuous occurrence of *Neogloboquadrina humerosa* is recorded from 3230 m. The FAD of *N. humerosa* is placed within

biozone MMi12 (Iaccarino et al., 2007), in agreement with the identification of this biozone in the Benicarlo C1 well (Fig. 6). A similar comment can be expressed for *Globigerinoides extremus*, which has been continuously recorded in the Benicarlo C1 well between 3220 m and 2900 m, that is also conceivable with the FAD of the species at the base of biozone MMi12 (Iaccarino et al., 2007).

The occurrence of *Globorotalia conomicoza* from 3110 to 2640 m characterizes the MMi13 biozone ending at 5.97 Ma (Iaccarino et al., 2007). Then, *Globorotalia margaritae* and *Sphaeroidinellopsis paenedehiscens* are recorded together from 2535 m, indicating the biozones MPI1-MPI2 up to the first record of *Globorotalia puncticalata* at 2511 m indicating the base of biozone MPI3 (Iaccarino et al., 2007). Finally, the uppermost record of *Globorotalia margaritae* at 2370 m is used to delimit the top of biozone MPI3, dated at 3.80 Ma. These data are transferred to Fig. 6 where the ages of the biozone boundaries are also indicated according to Iaccarino et al. (2007). It is thus obvious that an important portion of the deposits drilled at Benicarlo C1, more precisely those

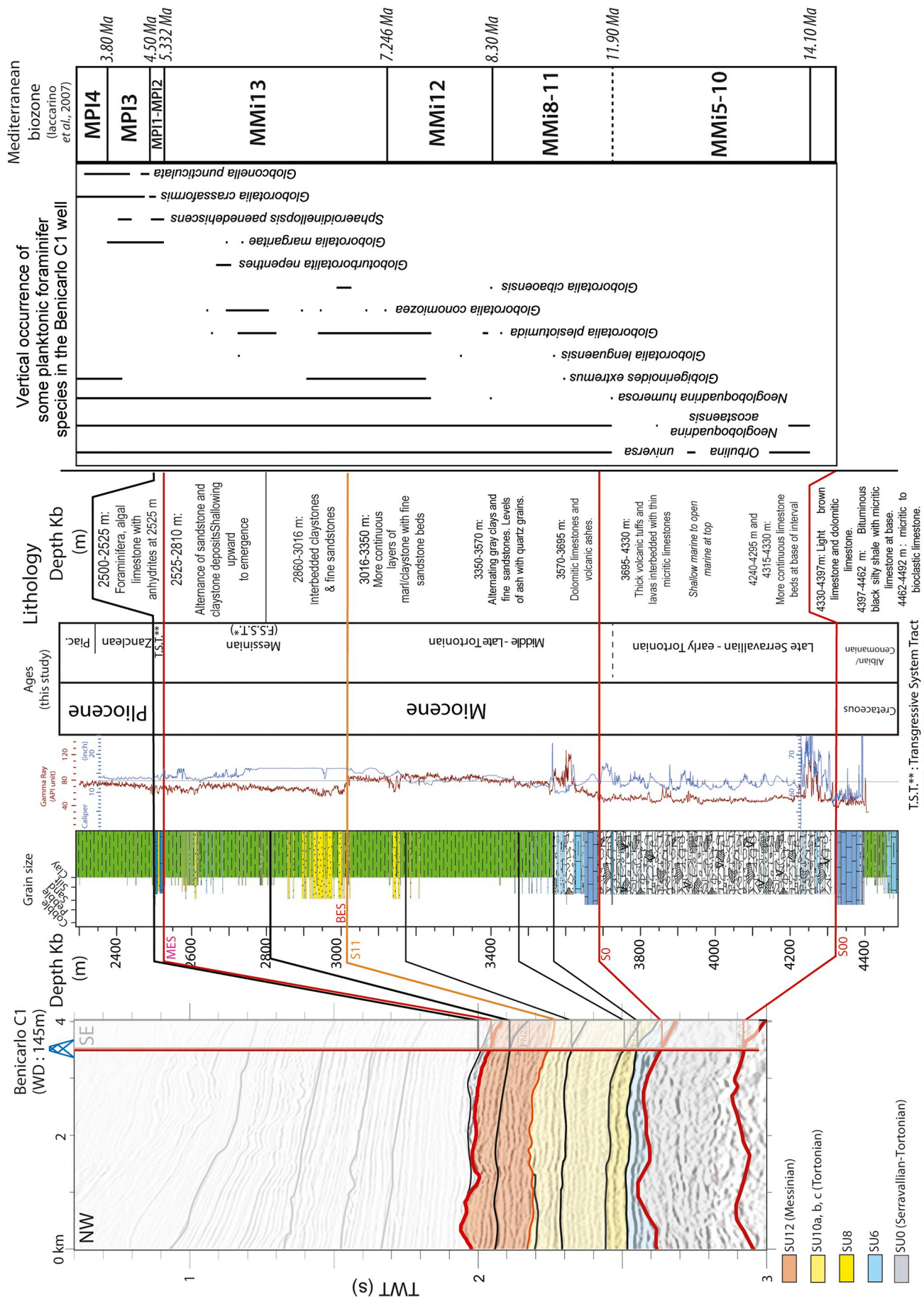


Fig. 6. Correlation of seismic units and Well Benicarlo C1, for the Miocene to Pliocene deposits. (Borehole position is shown on Figs. 1 & 2). The right part of the figure shows the vertical records of the concerned species, the horizontal lines indicate which level has been considered as corresponding to the first or last appearance datum (FAD or LAD) of some of them. Biozones and related ages refer to Gradstein et al. (2012). Caliper (blue curve) and Gamma Ray (red curve) are represented. (For interpretation of the references to colour in this figure legend, the reader is referred to the web version of this article.)

between 3110 m and 2511 m depth, belongs to the pre-evaporitic phase of the Messinian.

3.2.2. Lithologies and Environments

The very thick sequence of volcanic tuffs and lavas between 4315 m - 3730 m were deposited in a fairly shallow marine environment during late Serravallian-Early Tortonian time as shown by the thin interbeds of soft limestones containing rare *Amphistegina* sp. and planktonic foraminifera (Evans et al., 1978).

The sequence between 3695 and 3016 m, of Tortonian age is of open marine, outer sublittoral to bathyal nature. The onset of colder water conditions over this interval is shown by the presence of sinistral coiled specimens of *Globorotalia acostaensis* (since around 3400 m) before the warmer Messinian period (Suc et al., 1995; Evans et al., 1978).

The interval 2810–2525 m represents a shallowing upward phase, with the probable formation of underwater supra-littoral conditions at the top. The reduction in planktonic foraminifera and the upward coarsening of the sediments suggests a general shallowing of the basin at this time.

The interval between 2525 and 2500 m can be separated in two parts: the topmost part of this interval between approximately 2510–2500 m as well as interval 2525–2524 m contain thin beds of white algal limestone interbedded with white sandstone and yellow to ochre marl/claystone. The lower limestone contains anhydrite. Additionally, the occurrence of a single cyprid ostracod, algae and bryozoan in the 2515 and 2525–2520 m ditch cuttings sample is taken to indicate both a stratigraphic and environmental break at this level and possibly reflects the establishment of brackish - non-marine conditions (Evans et al., 1978).

The interval 2500–2370 m is characterized by soft, light grey calcareous shales and marls/claystone with minor sand stringers throughout. This interval is assigned to the Ebro Group, Early Pliocene, deposited in an open marine environment.

4. Discussion

4.1. Age assignment and sequence stratigraphic interpretation

Combining the results from seismic interpretation in correlation with biostratigraphy from Benicalo C1 well, we consider that the Messinian is represented mostly by marine sediments from 3016 to 2525 m depths, i.e. 491 m in thickness with a shallowing upward trend (Fig. 6). The proximal to distal correlation of seismic units SU12a to SU12c (both topped by the MES-S20) also shows a downward-shift of uppermost surface (as seen on depth-converted seismic transect shown in Fig. 3 and in backstripped section (Supplementary material 2).

The MES(-S20) is depicted as the maximum regressive surface (MRS in the sense of Catuneanu et al., 2011) and is located at 2525 m in the Benicalo C1 well. This MRS (MES) would be dated at 5.6 Ma according to Clauzon et al. (1996, 2015) and CIESM (2008). The underlying Messinian sediments (SU12a and SU12c) therefore correspond to the remaining sediments of the Falling Stage System Tract (FSST). According to our seismic interpretation, the erosive surface at the base (S11) may correspond to the regressive surface of marine erosion during the falling stage of the MSC crisis, also described in Quaternary sequences related to 100,000 years cycles (Rabineau et al., 2005). However, some early pre-MSC Messinian sediments seem to be preserved as biostratigraphic data suggest with the presence of *Globorotalia Cibaoensis* around 3000 m but considering the relative Messinian sea level fall velocity and amplitude, earlier pre-MSC deposits are very fortunate to be reworked and preserved in MSC related deposits.

This interpretation of the FSST for SU12a is supported by the fact that Benicalo C1 – shows sediments of a younger age than those found in both Fornax-1 and Tarragona E2 wells (Evans et al., 1978; Bessais and Cravatte, 1988; Urgeles et al., 2011) as well as a progressive downward shift of MES-S20 surface. Our seismic interpretation and correlation

suggest that SU12c is also part of this FSST and in fact represent the end of it with the most distal regressive deposits. Development of SU12c unit is followed by the initiation of the LU as lowstand system tract (in the sense of Boyd et al., 2006; Gorini et al., 2015) (Fig. 8, stage 3). This FSST and LST would correspond to the MLM (Messinian Lower Mega-sequence) of Gorini et al. (2015).

Unfortunately, no well exists to sample this unit SU12c, so we have no direct related biostratigraphic information, which could confirm or invalidate this hypothesis.

Above the MES at Benicalo C1, the occurrence of a single cyprid ostracod, algae and bryozoan in the 2515 m and 2525–2520 m cuttings suggest that this thin unit going from probable emersion to shallow water environments records the end of the MSC. Following CIESM (2008) or Bache et al. (2012) scenarios, this unit could be interpreted as corresponding to those deposited during the early marine reflooding of the Mediterranean Basin (Transgressive System Tract) that preceded the base of the Zanclean, and estimated between 5.46 and 5.33 Ma. This TST is overlain by a clear open-marine high stand System Tract (HST) with warm conditions in early Zanclean Pliocene. (5.33–3.85 Ma) (Suc et al., 1995).

4.2. Subaerial versus submarine erosion and position of the Messinian shoreline

Erosional surfaces may develop in subaerial or submarine environments. However, process and formation of erosional surfaces differ in the air and under water, due to the varying physics of the different fluids. In subaerial environments topography is highly variable. Landscapes are carved by rivers and strongly dependent on precipitation that will erode and transport sediment as a function of gravity and slopes as the primary controls. In submarine environments, widespread erosion also occurs: both in proximal environments (at the shoreline and on the shelf) with a strong impact of waves, tides and currents but also in deep environments such as submarine canyons, slopes and deep-sea areas with processes such as turbidity currents, landslides, debris flows (e.g. Amblas et al., 2006) and contour currents (e.g. Rebasco et al., 2014). In shallow environments (between 0 and 100 - 150 m) a very efficient erosion process is related to wave action. The main result of this wave action is the creation of large smooth morphologies and wave-cut terraces that are recognized worldwide throughout the geological time scale (e.g. Cattaneo and Steel, 2003; Catuneanu, 2006; Bache et al., 2014).

In our case study, S11 marks the first MSC regressive surface of marine erosion (RSME) prior to the MES development (see also above) and highlights Km₂ at an onshore-offshore position (Goswani et al., 2017). The overlying U12a clineforms (VB area) correspond to the Messinian forced-regressive prisms (FSST), with erosion and redeposition of sediments in the forced-regressive prisms (Fig. 4, section g; Fig. 6) and a MRS at the top.

The subaerial development of the Trans-VB incised-valley system is attested across the Tortosa-Ebro domain with rugged badland-type morphology, terraces, fluvial meanders, oxidation surfaces (Fornax-1) as fully explained in (Urgeles et al., 2011; Cameselle et al., 2014).

Moreover, as shown in the results section: the general slope of backstripped MES-S20-S21 erosional surface is only 0.55% (0.32°) or even less in segments between knickpoints (0.23° to 0.26°). These slope gradients are much smaller than any present-day well-defined submarine canyon. In the GOL, the shelf-break occurs when slope gradients reach 1%. Gradients < 1% delimit the continental shelf, whereas gradients > 1% correspond to the upper slope. The values obtained for the Messinian MES-S20-S21 are typical of low shelf gradients and not slope gradients where submarine canyons occur, they are generally between 2 and 5° in canyon head areas in the GOL (Baztan et al., 2005). Another example is provided by present-day submarine canyons in the VB that all show slopes around 10° in upper slope submarine canyons to 2–4° at the base of slope canyons (Amblas et al., 2006). Those values are more

than one order of magnitude higher than what we measured here. MES-S20 general shape cannot be related to any submarine canyon mechanism.

If MES-S20 might have been also initiated as submarine one, this composite erosive surface was then re-worked as a subaerial surface of erosion related to the Messinian lowermost sea level (MRS) with a coastline that reached at least km₃ (270 km; Fig. 3 Transect 01). Its outlet is associated with the development of SU12c after the Km₃ knickpoint and the start of S11c erosional surface at its base. The limit of prograding SU12c unit would thus correspond to the most distal detritic products related to the relative MSC sea level fall stage.

The Messinian shoreline (Fig. 3 Transect 01; Fig. 5, section I and Supplementary material 2) existed at least up to km 270. In any event, the minimum lowest MSC sea level (at km₃) was around −1100 m below present day sea-level according to the backstripped section, SU12c corresponds to the final development of the detritic product related to the MSC sea-level fall. The values we give here for sea-level reconstruction are probably maximum values as backstripping was conducted up to 5.3 Ma after the UU deposition (and not 5.6 Ma at the maximum sea level drawdown).

4.3. A model for the Messinian Ebro incised-valley formation: segmentation, knickpoint role, and palaeogeographic implications

The model in Fig. 7 attempts to explain the Ebro paradox and the following scenario, which highlights the multiple versus single knickpoint model implication in the fluvial dynamic during relative sea-level change. From this simplified model, identification of a 270 km long Messinian Ebro incised-valley system and its infilling by detrital FSST deposits allows us to propose an explanation clarifying the relationship between drainage areas and the Messinian fluvial incision.

The existence of a pre-Messinian physiography and segmentation in the Valencia Basin (Pellen et al., 2016) plays a crucial role in its subsidence history, with an induced pre-Messinian step-by-step seafloor deepening between the sagged VB, the MB and the deep LPB (Figs. 7 & 8a, stage 1).

Prior to the MSC sea level fall, the gradual restriction of the marine connections (CIESM, 2008; Roveri et al., 2014) would imply relative minor sea level variation. As a fact a first retrogressive erosion Km₁ is located at the CCR area, following the principle of the river equilibrium profile (Miall, 2013). The result is the initiation of S11 basal erosive surface at the platform edge (Km₂) (Fig. 8a, Stage 1) and the detrital sediment deposition (SU12a) offshore fluvial systems.

The progressive limitation of exchanges followed by the abrupt break of water exchanges through the Rifian strait (Krijgsman et al.,

1999) at 5.60 Ma resulted in a rapid sea-level fall within the Mediterranean Basin. The sea level quickly reached Km₂ (Fig. 8a, Stage 2a) implying a shift to the outermost limit of the Miocene platform of the main retrogressive erosion. The eroded products were gradually deposited along the former Miocene slope area, forming the SU12a unit (as drilled in Benicalo well and showing ages of at least 6.14 to 5.72 Ma). With the sea-level fall continuing, up to 5.6–5.45 Ma depending on the chronostratigraphy of the discussed scenarios (i.e. CIESM, 2008; Bache et al., 2012, 2015; Gorini et al., 2015), the main regressive erosion shifted again and the upper part of S12a was partially reworked and redeposited in the offshore domain as in FSST or Forced regression models (Gorini et al., 2015). Little detrital SU12a formation is observed at the VB base of slope because, between stage 2a and 2b (Fig. 8a), the accommodation space in the Valencia foot slope area was too small to accumulate thick series. This implies intense sedimentary transfer from the subaerial eroded platform domain directly to the deep marine Menorca and Provence domains. When the sea level reached Km₃, the fluvial base-level and main retrogressive erosion migrated to the Valencia-Menorca transition with clear erosional truncations (Fig. 8a, stage 2b) and the detrital sedimentation was transferred to the Menorca and Provence deep domain, as shown by the development of the SU12c prograding clinoforms. At the lowest sea-level, our interpretations locate the shoreline at Km₃, observed on the CFZ axis (Fig. 3).

This evolution of downward shift erosion and the clear shift of the depocentres towards the deep basin is typical of a falling stage system tract that occurs on rather flat areas separated by steps which involve a proximal regressive erosion together with a distal retrogressive erosion at the step (knickpoint). As the sea-level fall continues, we observe a quick shift of this double erosion from Km₁ to Km₃. With this mechanism, the river equilibrium profile has to be well developed at Km₃ so as to observe major retrogressive erosional process at Km₂ area. Depending of the inertia of the retrogressive erosion dynamics at each knickpoint, there is no increased fluvial erosion nor propagation towards the onshore Ebro areas as in the case of the Rhône (see below). The existence of the CCR may also further prevent the propagation of the fluvial erosion towards the inner parts of the EB.

In the Rhone system, earlier work showed the existence of three hinge lines in between different structural domains related to the opening of the LPB. The model in Fig. 8b (stage 1–4) illustrates the development of Messinian Pyrenean-Languedocian and Rhone fluvial systems during the MSC sea-level drop, based on the work of Bache et al. (2009), Bache et al. (2010, 2012, 2015) and Gorini et al. (2015). Domain 2b corresponds to the main geodynamic sill which records the gradual transition between marine and aerial domain during the MSC sea-level fall (5.6–5.55 Ma) i.e. Gorini et al., 2015 and slow sea-level rise (formation of wave ravinement erosion surface between 5.55 and 5.46 Ma if we follow Bache et al., 2012 scenario). Only minor onshore knickpoints are mapped along the Rhone fluvial profile (Clauzon, 1982), and the main knickpoint is therefore located at the hinge line 2 (the shelf-break) which also corresponds to the first development of forced falling stage system tract of the MSC (Leroux et al., 2015a, 2015b). The model highlights the initiation of retrogressive erosion at the second geodynamic knickpoint (the shelf break), which quickly progresses landward from the former Miocene shelf-edge to the edge of the Central Massif (Pyrenean-Languedocian rivers) or along the Rhone-Bresse valley (Fig. 8b, stage 1–3) up to Lyon city.

Domain 2a (GOL) can be compared to the VB basin area/VB-MB transition, which records the lowest MSC base-level and early relative sea-level rise. Around the Km₃ area, a minimum of four successive marine incisions are observed in the UU deposits (Fig. 3, section e), implying (1) a composite refilling for the trans-VB valley system and (2) preservation of the latter in the sense of Boyd et al. (2006). If the UU are mainly developed along the main channel (~0.3 twt thick) few deposits are observed on both sides of the channel, involving a partial/complete reshaping of S20 erosional surface. This observation may be related to

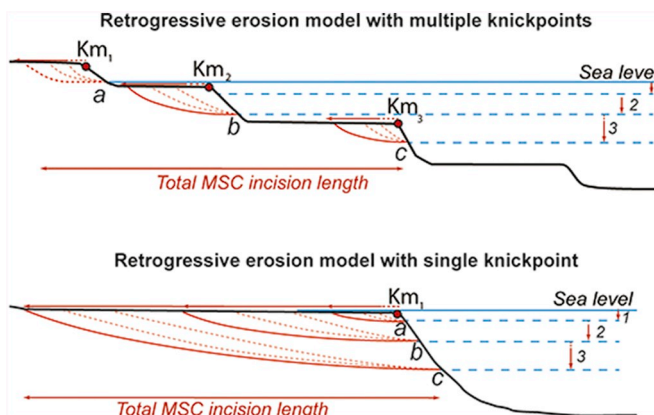


Fig. 7. Simplified schematic section illustrating the role of multiple versus single knickpoints in retrogressive erosion response during a relative sea level fall. a, b, c correspond to the rejuvenation phase of the retrogressive erosion linked to the relative sea level successive falls (step 1, 2, 3).

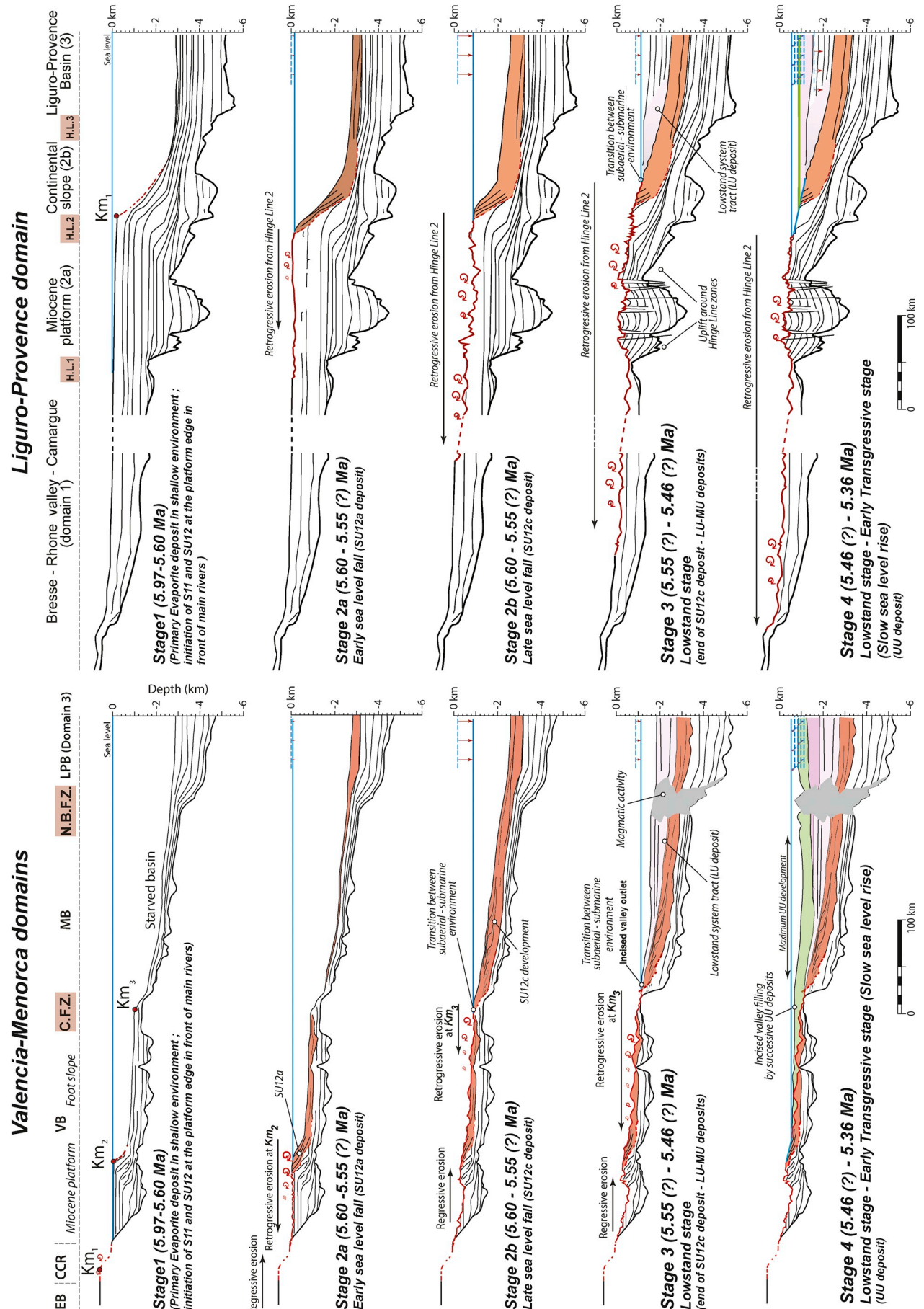


Fig. 8. Schematic and balanced cross section of the VB-MB (Fig. 8a) and LPB (Fig. 8b) illustrating the impact of sills and sea-level drop on the fluvial valley system development and paleo-depositional profile process during the Messinian event. During sea-level drop, erosion occurs both as regressive erosion of the fluvial system but also as retrogressive erosion from more distal knickpoints (see text for further explanation).

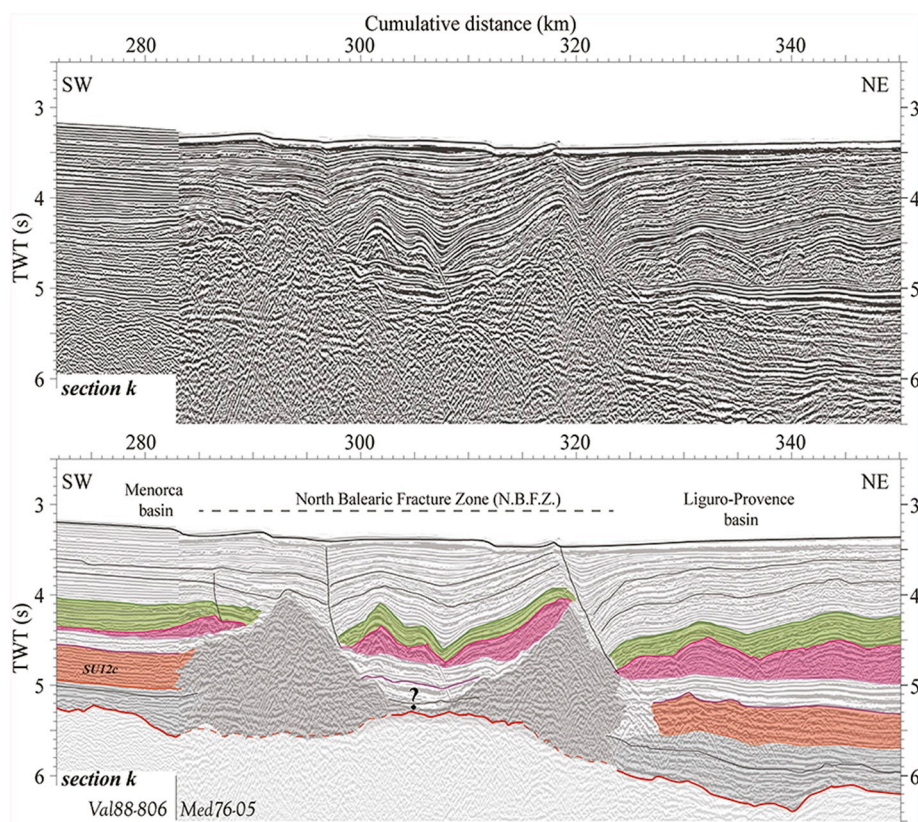


Fig. 9. Detailed seismic section highlighting the magmatic pulse during the Lower Unit deposition and Pliocene-Quaternary time at the Menorca Basin and Liguro-Provence Basin transition (North Balearic Fracture Zone area) (Location and units colour code as in Figs. 4 & 5).

other morphological features, such as the general extent of the smooth surface along the Catalan and domain 2b of the LPB (Bache et al., 2009, Bache et al., 2012; Garcia et al., 2011; this study) (Fig. 6). This tends to favour a similar genesis during a relative slow sea-level rise (Fig. 8, stage 4), the rough surface being eroded by wave action (Cattaneo and Steel, 2003; Bache et al., 2012, 2015) and only preserved upstream by the later rapid sea-level rise closing the Messinian event.

We thus propose that domain 2b and VB basin area/VB-MB transition are equivalent morphological domains which both record the lowest MSC sea-level. Significant lateral spacing between each morphological knickpoint has provided better stratigraphic and morphological observation for the VB. As the VB record the whole Messinian palaeo-Ebro incised valley, the Ebro paradox disappears if the length of Messinian rivers are measured from MSC paleo-shorelines at the CFZ area, and not from pre-Messinian or present-day shorelines (Fig. 7).

At the MSC paroxysm, the trans-VB incised valley system watershed would include the Valencia Basin and its borders ($55,000 \text{ km}^2$; including the Betic-influenced southwest area, its mountainous borders (southern part of the Catalan Range) and at least the eastern part of the Ebro Basin ($? < \text{Ebro watershed} < 85,000 \text{ km}^2$). However, our result cannot confirm or infirm a pre-Messinian proto-Ebro hypothesis. Stratigraphic and thermochronological interpretations path suggest a pre-Messinian opening of the Ebro Basin (Fillon et al., 2013; Canals et al., 2013) with a single proto-Ebro river or multiple mountainous rivers cutting across the CCR. These models need to be confirmed by an assessment of offshore sedimentary volumes during Miocene, Messinian and Pliocene-Quaternary times that would lead to a better estimate of the paleo-drainage area evolution before/after the opening of the EB.

The NBFZ sill is overloaded by igneous pulses starting during the LU deposition and during Pliocene-Quaternary time (Fig. 9; this was also observed onshore by Martí et al., 1992; Araña et al., 1983). Recent studies have linked this Messinian magmatic pulse to the Messinian desiccation (Sternai et al., 2017) or to a more global kinematic re-

organization (Leroux et al., 2018). Whatever the lithospheric processes implied, the Ebro incised-fluvial system constrained by the CCR and by the CFZ confirms the strong influence of VB-MB-LPB margin structural segmentation on the development of the Messinian Ebro fluvial system, and more generally on the whole Neogene sedimentological evolution.

5. Conclusion

Extending the Cameselle et al. (2014) results, we have identified and characterized along the Valencia, Menorca and towards Liguro-Provence basins a 270 km long Messinian fluvial valley-incision – from the Messinian shoreline to the CCR – as well as the spatial distribution of the related distal detrital deposits. The Ebro Messinian erosional system now displays the same order of incised river length as the Rhone, resolving the paradoxical relationship between the present-day fluvial drainage area and the Messinian fluvial system of Babault et al. (2006). Following our interpretation, the Ebro Basin and Mediterranean Sea were connected at least at the MSC sea-level drop. Only detailed sedimentary fluxes analysis could confirm or infirm a pre-Messinian connection between the Ebro Basin and the Mediterranean Sea.

The segmentation and nature of the substratum triggered the formation of knickpoints due to differential subsidence between the shallow VB, the transitional MB and the deep LPB, and controlled fluvial processes and erosion during the MSC sea-level drop. These knickpoints induced step-by-step major regressive-retrogressive fluvial erosional processes which shift through time during sea-level drop. This work highlights the general major relationship between kinematic, subsidence evolution, base-level fall and depositional response particularly well expressed during the outstanding Messinian Salinity Crisis event.

Supplementary data to this article can be found online at <https://doi.org/10.1016/j.gloplacha.2019.102988>.

Acknowledgments

This work was co-funded by a grant from the French government under the program “Investissements d’Avenir” the “Laboratoire d’Excellence” LabexMER (ANR-10-LABX-19), and ISBLUE (ANR-17-EURE-0015) and by a grant from the Regional Council of Brittany. It was further supported by CNRS and IFREMER, with additional support from the French Actions-Marges Program (JL Rubino & P. Unternehr) and the GRI Méditerranée (Groupe de Recherche et Industrie TOTAL-UPMC). The Data base was built thanks to the SIGEOF spanish site, to academic cruises from France including PROGRES, AM-MED-1 (Leg 1 and Leg2), SARDINIA, WESTMEDFLUX, SEEPGOL, VALSIS) and Spain. We wish to thank TOTAL and Schlumberger for giving access to the seismic data and well data used in this study. The biostratigraphic studies and re-evaluations were performed by biostratigraphers from TOTAL. The authors acknowledge the fruitful and constructive reviews by Antonio Pedrera, Agnes Maillard, Lluís Cabrera and Dennis Brown, as well as those from the editor Liviu Matenco that greatly improved the manuscript.

References

- Afilhado, A., Moulin, M., Aslanian, D., Schnürle, P., Klingelhoefer, F., Nouzé, H., Rabineau, M., Leroux, E., Beslier, M.-O., 2015. Deep crustal structure across a young passive margin from wide-angle and reflection seismic data (the SARDINIA Experiment) – II. Sardinia’s margin. *Bull. Soc. Géol. France* 186, 331–351.
- Amblas, D., Canals, M., Urgeles, R., Lastras, G., Liqueite, C., Hughes-Clarke, J.E., Casamor, J.L., Calafat, A.M., 2006. Morphogenetic mesoscale analysis of the northeastern Iberian margin, NW Mediterranean Basin. *Mar. Geol.* 234, 3–20.
- Amblas, D., Gerber, T.P., Canals, M., Pratson, L.F., Urgeles, R., Lastras, G., Calafat, A.M., 2011. Transient erosion in the Valencia Trough turbidite systems, NW Mediterranean Basin. *Geomorphology* 130 (3–4), 173–184.
- Araña, V., Aparicio, A., Martín Escorza, C., García Cacho, L., Ortiz, R., Vaquer, R., Barberi, F., Ferrara, G., Albert, J., Gassiot, X., 1983. El volcanismo neogeno-cuaternario de Catalunya: características estructurales, petrologicos y geodinámicos. *Acta Geol. Hisp.* 28, 1–17.
- Arche, A., Evans, G., Clavell, E., 2010. Some considerations on the initiation of the present SE Ebro river drainage system: Post- or pre-Messinian? *J. Iber. Geol.* 36 (1), 73–85.
- Babault, J., Loget, N., Van Den Driessche, J., Castelltort, S., Bonnet, S., Davy, P., 2006. Did the Ebro basin connect to the Mediterranean before the Messinian salinity crisis? *Geomorphology* 81, 155–165.
- Bache, F., 2008. Evolution Oligo-Miocène des marges du micro océan Liguro-Provençal. Thèse d’Etat: Université de Bretagne Occidentale, Brest, pp. 1–328.
- Bache, F., Olivet, J.L., Gorini, C., Rabineau, R., Baztan, J., Aslanian, D., Suc, J.P., 2009. Messinian erosional and salinity crises: view from the Provence basin (Gulf of Lions, Western Mediterranean). *Earth and Planetary Science Letters* 286, 139–157.
- Bache, F., Olivet, J.L., Gorini, C., Aslanian, D., Labails, C., Rabineau, M., 2010. Evolution of rifted continental margins: the cases of the Gulf of Lions (western Mediterranean basin). *Earth Planet. Sci. Lett.* 292, 345–356.
- Bache, F., Popescu, S.-M., Rabineau, M., Gorini, C., Suc, J.-P., Clauzon, G., Olivet, J.-L., Rubino, J.-L., Melinte-Dobrescu, M.C., Estrada, F., Londeix, L., Armijo, R., Meyer, B., Jolivet, L., Jouannic, G., Leroux, E., Aslanian, D., Dos Reis, A.T., Mocochain, L., Dumurdžanov, N., Zagorčev, I., Lesić, V., Tomić, D., Çağatay, M.N., Brun, J.-P., Sokoutis, D., Csato, I., Ucarkus, G., Çakir, Z., 2012. A two-step process for the re-flooding of the Mediterranean after the Messinian Salinity Crisis. *Basin Res.* 24, 125–153.
- Bache, F., Sutherland, R., King, P.R., 2014. Use of ancient wave-ravinement surfaces to determine paleogeography and vertical crustal movements around New Zealand. *N. Z. J. Geol. Geophys.* 57, 459–467.
- Bache, F., Gargani, J., Suc, J.-P., Gorini, C., Rabineau, M., Popescu, S.M., Leroux, E., Do Couto, D., Jouannic, G., Rubino, J.-L., Olivet, J.-L., Clauzon, G., Dos Reis, A., Aslanian, D., 2015. Messinian evaporite deposition during sea level rise in the Gulf of Lion (Western Mediterranean). *Mar. Pet. Geol.* 66, 262–277.
- Bailey, H.W., Gallagher, L., Woodhouse, B., 2008. Biostratigraphy of the Well Fornax Offshore, Spain. (12 pp. Unpublished biostratigraphic report).
- Balázs, A., Granjeon, D., Matenco, L., Szánató, O., Cloetingh, S., 2017. Tectonic and climatic controls on asymmetric half-graben sedimentation: inferences from 3-D numerical modelling. *Tectonics* 36, 2123–2141.
- Bartrina, M.T., Cabrera, L.L., Jurado, M.J., Guimera, J., Roca, E., 1992. Cenozoic evolution of the central Catalan margin (Valencia Trough, Western Mediterranean). *Geology and Geophysics of the Valencia Trough, Western Mediterranean*. *Tectonophysics* 203, 219–248.
- Baztan, J., Berné, S., Olivet, J.-L., Rabineau, M., Aslanian, D., Gaudin, M., Réhault, J.-P., Canals, M., 2005. Axial incision: the key to understand submarine canyon evolution (in the western Gulf of Lion). *Mar. Pet. Geol.* 22 (6–7), 805–826.
- Bessais, E., 1984. Etude palynologique du Pliocène du sondage Tarragona E2. Rapport de stage D.E.A. Univ. Sc. Tech. Languedoc, Montpellier (21 pp.).
- Bessais, E., Cravatte, J., 1988. Pliocene Vegetational ecosystems in South Catalonia, latitudinal variations in the Northwest Mediterranean Region. *Geobios* 21, 49–63.
- Boyd, R., Dalrymple, R.W., Zaitlin, B.A., 2006. Estuarine and Incised-Valley facies model. *SEPM Spec. Publ.* 84, 171–235.
- Cameselle, A.L., Urgeles, R., 2015. Large-scale margin collapse during Messinian early sea-level drawdown: the SW Valencia trough, NW Mediterranean. *Basin Res.* 29 (S1), 576–595.
- Cameselle, A.L., Urgeles, R., De Mol, B., Camerlenghi, A., Canning, J.C., 2014. Late Miocene sedimentary architecture of the Ebro Continental Margin (Western Mediterranean): implications to the Messinian Salinity Crisis. *Int. J. Earth Sci. (Geol. Rundsch.)* 1–18.
- Canals, et al., 2013. Integrated study of Mediterranean deep canyons: novel results and future challenges. *Prog. Oceanogr.* 118, 1–27.
- Cattaneo, A., Steel, R.J., 2003. Transgressive deposits: a review of their variability. *Earth Sci. Rev.* 62, 187–228.
- Catuneau, 2006. Principles of Sequence Stratigraphy. The Netherlands, Elsevier, Amsterdam (375 pp.).
- Catuneau, O., Galloway, W.E., Kendall, C.G.S.C., Miall, A.D., Posamentier, H.W., Strasser, A., Tucker, M.E., 2011. Sequence stratigraphy: methodology and nomenclature. *Newsl. Stratigr.* 44 (3), 173–245.
- CIESM, 2008. In: Briand, F. (Ed.), The Messinian Salinity Crisis from Mega-Deposits to Microbiology – A Consensus Report. N° 33 in CIESM Workshop Monographs. CIESM Publisher, Monaco (168 pp.).
- Clauzon, G., 1982. Le canyon Messinien du Rhône: une preuve décisive du “desiccated deep-basin model” (Hsü, Cita and Ryan, 1973). *Bull. Soc. Géol. Fr.* 24 (3), 597–610.
- Clauzon, G., 1999. L’impact des variations eustatiques du bassin de Méditerranée occidentale sur l’orogène alpin depuis 20 Ma (In French). *Etudes Géogr. Phys.* 28, 33–40.
- Clauzon, G., Suc, J.-P., Gautier, F., Berger, A., Loutre, M.-F., 1996. Alternate interpretation of the Messinian salinity crisis: controversy resolved? *Geology* 24, 363–366.
- Clauzon, G., Suc, J.-P., Do Couto, D., Jouannic, G., Melinte-Dobrescu, M.C., Jolivet, L., Quillévér, F., Lebret, N., Mocochain, L., Popescu, S.-M., Martinell, J., Doménech, R., Rubino, J.-L., Gumiaux, C., Warny, S., Bellas, S.M., Gorini, C., Bache, F., Rabineau, M., Estrada, F., 2015. New insights on the Sorbas Basin (SE Spain): the onshore reference of the Messinian Salinity Crisis. *Mar. Pet. Geol.* 66, 71–100.
- Clavell, E., Berastegui, X., 1991. Petroleum geology of the Gulf of Valencia. Generation, accumulation, and production of Europe’s hydrocarbons (Ed. A.M. Spencer). *Spec. Publ. Eur. Assoc. Petro. Geosci.* 1, 355–368.
- Costa, E., Garcés, M., Lopez-Blanco, M., Beamud, E., Gomez-Paccard, M., Larrasoña, J.C., 2010. Closing and continentalization of the south Pyrenean foreland basin (NE Spain): magnetostratigraphic constraints. *Basin Res.* 22, 904–917.
- Cravatte, J., 1980. Etude microstratigraphique du Miocène et essai de corrélations entre les forages de Te-2, Garraf 1, BMB-1, BMC-1 et BME-1: Rapport confidentiel, total Direction fonctionnelle Exploration. Département Laboratoires Exploration, pp. 1–16.
- Del Olmo, W.M., 2011. The Messinian in the Gulf of Valencia and Alboran Sea (Spain): paleogeography and paleoceanography implications. *Rev. Soc. Geol. Esp.* 24, 1–22.
- Escutia, C., Maldonado, A., 1992. Paleogeographic implications of the Messinian surface in the Valencia trough, northwestern Mediterranean Sea. In: Banda, E., Santanach, P. (Eds.), *Geology and Geophysics of the Valencia Trough, Western Mediterranean*. *Tectonophysics* 203, 263–284.
- Etheve, N., Frizon de Lamotte, D., Mohn, G., Martos, R., Roca, E., Blanpied, C., 2016. Extensional vs contractional Cenozoic deformation in Ibiza (Balearic promontory, Spain): integration in the West Mediterranean back-arc setting. *Tectonophysics* 682, 35–55.
- Etheve, N., Mohn, G., Frizon de Lamotte, D., Roca, E., Tugend, J., Gomez-Romeu, J., 2018. Extreme Mesozoic Crustal thinning in the eastern Iberia margin: the example of the Columbretes basin (Valencia trough). *Tectonics* 37 (2), 636–662.
- Evans, D.J., Peter, C.K., Price, R.J., 1978. Biostratigraphy and Depositional Environments Over the Internal 450 m to 4492 m (T.D.), Together With Petrographic Descriptions of Samples Between 3620 m to 4190 m in the Union Texas Espana Inc. Benicalo C-1 well, Offshore Spain. Robertson Research (North America) Limited (unpublished Exploration Report n° 194, 61 pp.).
- Fillon, C., Gautheron, C., van der Beek, P., 2013. Oligocene–Miocene burial and exhumation of the Southern Pyrenean foreland quantified by low-temperature thermochronology. *J. Geol. Soc.* 170, 67–77.
- Flcker, R., Krijgsman, W., Capella, W., de Castro Martins, C., Dmitriev, E., Mayser, J.P., Marzocho, A., Modest, S., Ochoa, D., Simon, D., Tulbere, M., van der Berg, B., van der Schee, M., de Lange, G., Ellam, R., Govers, R., Gutjahr, M., Hilgen, F., Kouwenhoven, T.J., Lofi, J., Meijer, P., Sierro, F.J., Bachiri, N., Barhoum, N., Alami, A.C., Chacon, B., Flores, J.A., Gregory, J., Howard, J., Lunt, D., Ochoa, M., Pancost, R., Vincent, S., Yousfi, M.Z., 2015. Evolution of the Late Miocene Mediterranean–Atlantic gateways and their impact on regional and global environmental change. *Earth Sci. Rev.* 150, 365–392.
- Frey-Martinez, J., Cartwright, J.A., Burgess, P.M., Vicente-Bravo, J., 2004. 3D seismic interpretation of the Messinian Unconformity in the Valencia Basin, Spain: 3D seismic Technology: Application to the Exploration of Sedimentary Basins. (Ed. by R.J. Davies, J.A. Cartwright, S.A. Stewart, M. Lappin & J.R. Underhill). *Mem. Geol. Soc. Lond.* 29, 91–100.
- Garcia, M., Maillard, A., Aslanian, D., Rabineau, M., Alonso, B., Gorini, C., Estrada, F., 2011. The Catalan margin during the Messinian Salinity Crisis: Physiography, morphology and sedimentary record. *Mar. Geol.* 284, 158–174.
- Garcia-Castellanos, D., Larrasoña, J.C., 2015. Quantifying the post-tectonic topographic evolution of closed basins: the Ebro basin (Northeast Iberia). *Geology* 43 (8), 663–667.
- Gorini, C., Montadert, L., Rabineau, M., 2015. New imaging of the salinity crisis: dual Messinian lowstand megasequences recorded in the deep basin of both the eastern and western Mediterranean. *Mar. Pet. Geol.* 66, 1–17.
- Goswani, R., Mitchell, N.C., Brocklehurst, S.H., Argnani, A., 2017. Linking subaerial

- erosion with submarine geomorphology in the western Ionian Sea (south of the Messina Strait), Italy. *Basin Res.* 29, 641–658.
- Gradstein, F.M., Ogg, J.G., Schmitz, M.D., Ogg, G.M. (Eds.), 2012. The Geological Time Scale 2012. Elsevier, Amsterdam (1144 pp.).
- Grimaud, J.-L., Paola, C., Voller, V., 2016. Experimental migration of knickpoints: influence of style of base-level. *Earth Surf. Dyn.* 4, 1–11.
- Gueguen, E., Doglioni, C., Fernandez, M., 1998. On the post-25 Ma geodynamic evolution of the western Mediterranean. *Tectonophysics* 298, 259–269.
- Guennoc, P., Gorini, C., Mauffret, A., 2000. Histoire géologique du Golfe du Lion et cartographie du rift oligo-aquitainien et de la surface messinienne. *Géol. Fr.* 3, 67–97.
- Helland-Hansen, W., Hampson, G., 2009. Trajectory analysis: concepts and application. *Basin Res.* 21 (5), 454–483.
- Hunt, D., Tucker, M.E., 1992. Stranded parasequences and the forced regressive wedge systems tract: deposition during base-level fall. *Sediment. Geol.* 81, 1–9.
- Iaccarino, S., Premoli Silva, I., Biolzi, M., Foresi, L.M., Lirer, F., Turco, E., Petrizzi, M.R., 2007. In: Biolzi, M., Iaccarino, S., Turco, E., Checconi, A., Rettori, R. (Eds.), Practical Manual of Neogene Planktonic Foraminifera. Univ. Perugia-Parma-Milano (131 pp.).
- Jolivet, L., Gorini, C., Smit, J., Leroy, S., 2015. Continental breakup and the dynamics of rifting in back-arc basins: the Gulf of Lion margin. *Tectonics* 34 (4) (2014TC003570).
- Krijgsman, W., Langereis, C.G., Zachariasse, W.J., Boccaletti, M., Moretti, G., Gelati, R., Iaccarino, S., Papani, G., Villa, G., 1999. Late neogene evolution of the Taza-Guerfir Basin (Rifian Corridor, Morocco) and implications for the Messinian salinity crisis. *Mar. Geol.* 153, 147–160.
- Leever, K.A., Matenco, L., Garcia-Castellanos, D., Cloetingh, S., 2010. The evolution of the Danube gateway between Central and Eastern Paratethys (SE Europe): Insight from numerical modelling of the causes and effects of connectivity between basins and its expression in the sedimentary record. *Tectonophysics* 502, 175–195.
- Leroux, E., Aslanian, D., Rabineau, M., Granjeon, D., Gorini, C., Droz, L., 2015a. Sedimentary markers in the Provençal Basin (western Mediterranean): a window into deep geodynamic processes. *Terra Nova* 27, 122–129.
- Leroux, E., Rabineau, M., Aslanian, D., Gorini, C., Bache, F., Moulin, M., Pellen, R., Granjeon, D., Rubino, J.-L., 2015b. Post-rift evolution of the Gulf of Lion margin tested by stratigraphic modelling. *Bull. Soc. Géol. France* 186, 291–308.
- Leroux, E., Rabineau, M., Aslanian, D., Gorini, C., Bache, F., Robi, C., Droz, L., Moulin, M., Poort, J., Rubino, J.-L., Suc, J.P., 2017. High-resolution evolution of terrigenous sediment yields in the Provence Basin during the last 6 Ma: relation with climate and tectonics. *Basin Research* 29, 305–339.
- Leroux, E., Aslanian, D., Rabineau, M., Pellen, R., Moulin, M., 2018. The late Messinian event: a worldwide tectonic upheaval. *Terra Nova* 30 (3), 207–214.
- Lirer, F., Iaccarino, S., 2011. Mediterranean Neogene historical stratotype sections and Global Stratotype Section and Points (GSSP): state of the art. *Ann. Naturhist. Mus. Wien* 113 (A), 67–144.
- Lofi, J., Sage, F., Deverchère, J., Loncke, L., Maillard, A., Gaullier, V., Thimon, I., Gillet, H., Guennoc, P., Gorini, C., 2011. Refining our knowledge of the Messinian Salinity crisis records in the offshore domain through multi-site seismic analysis. *Bull. Soc. Géol. France* 182, 163–180.
- Maillard, A., Mauffret, A., 1999. Crustal structure and rift genesis of the Valencia Trough (NW Mediterranean Sea). *Basin Res.* 11, 357–379.
- Maillard, A., Mauffret, A., 2006. Relationship between erosion surfaces and Late Miocene Salinity Crisis deposits in the Valencia Basin (Northwestern Mediterranean): evidence for an early sea-level fall. *Terra Nova* 18, 321–329.
- Maillard, A., Gorini, C., Mauffret, A., Sage, F., Lofi, J., Gaullier, V., 2006. Offshore evidence of polyphase erosion in the Valencia Basin (Northwestern Mediterranean): scenario for the Messinian Salinity Crisis. *Sediment. Geol.* 188–189, 69–91.
- Manzi, V., Gennari, R., Hilgen, F., Krijgsman, W., Lugli, S., Roveri, M., Siorro, F.J., 2013. Age refinement of the Messinian salinity crisis onset in the Mediterranean. *Terra Nova* 25, 315–322.
- Marti, J., Mitjavila, J., Roca, E., Aparicio, A., 1992. Cenozoic magmatism of the Valencia through (western Mediterranean): relationship between structural evolution and volcanism. *Tectonophysics* 203, 145–165.
- Mauffret, M.-A., Urgeles, R., Berné, S., Canning, J., 2017. Development of submarine canyons after the Mid-Pleistocene transition on the Ebroi margin, NW Mediterranean: The role of fluvial connections. *Q. Sci. Rev.* 158, 77–93.
- Miall, A.D., 2013. The Geology of Fluvial Deposits, 4th Corrected Printing. (581 pp.).
- Mitchum, R., Vail, P., 1977. Seismic stratigraphy and global changes of sea-level, part 7: Seismic Stratigraphic Interpretation Procedure - in Seismic Stratigraphy - applications to hydrocarbon exploration. In: Payton, C.E. (Ed.), AAPG Mem. 26, Tulsa, Oklahoma, USA.
- Moulin, M., Klingelhoefer, F., Afifhado, A., Aslanian, D., Schnurle, P., Nouzé, H., Rabineau, M., Beslier, M.-O., Feld, A., 2015. Deep crustal structure across a young passive margin from wide-angle and reflection seismic data (the SARDINIA Experiment) – I. Gulf of Lion's margin. *Bull. Soc. Géol. France* 186, 309–330.
- Olivet, J.L., 1996. La cinématique de la plaque Ibérique. *Bull. Centres Rech. Explor. Prod.*
- Elf-Aquitaine 20, 131–195.
- Palcu, D.V., Golovina, L.A., Vernyhorova, Y.V., Popov, S.V., Krijgsman, W., 2017. Middle Miocene paleoenvironmental crises in Central Eurasia caused by changes in marine gateway configuration. *Glob. Planet. Chang.* 158, 57–71.
- Pellen, R., Aslanian, D., Rabineau, M., Leroux, E., Gorini, C., Silenziario, C., Blanpied, C., Rubino, J.-L., 2016. The Menorca Basin: a buffer zone between the Valencia and Liguro-Provençal Basins (NW Mediterranean Sea). *Terra Nova* 00, 1–16.
- Pellen, R., Popescu, S.-M., Suc, J.-P., Melinte-Dobrescu, M.C., Rubino, J.-L., Rabineau, M., Marabini, S., Loget, N., Casero, P., Cavazza, W., Head, M.J., Aslanian, D., 2017. The Apennine foredeep (Italy) during the latest Messinian: Lago Mare reflects competing brackish and marine conditions based on calcareous nanofossils and dinoflagellate cysts. *Geobios* 50 (3), 237–257.
- Plint, A.G., 1988. Sharp-based shoreface sequences and “offshore bars” in the Cardium Formation of Alberta: their relationship to relative changes in sea level. In: Wilgus, C.K., Hastings, B.S. (Eds.), Sea-level Changes: an Integrated Approach. SEPM Special Publication No. 42, Tulsapp. 357–370.
- Rabineau, M., Berné, S., Aslanian, D., Olivet, J.-L., Joseph, P., Guillocheau, F., Bourillet, J.-F., Ledrezen, E., Granjeon, D., 2005. Sedimentary sequences in the Gulf of Lions: a record of 100,000 years climatic cycles. *Mar. Pet. Geol.* 22, 775–804.
- Rabineau, M., Leroux, E., Bache, F., Aslanian, D., Gorini, C., Moulin, M., Molliex, S., Droz, L., Reis, T.D., Rubino, J.-L., Olivet, J.-L., 2014. Quantifying subsidence and isostatic readjustment using sedimentary paleomarkers, example from the Gulf of Lion. *Earth Planet. Sci. Lett.* 388, 1–14.
- Rebesco, M., Hernandez-Molina, F.J., Van Rooij, D., Wahlin, A., 2014. Contourites and associated sediments controlled by deep-water circulation processes: state-of-the-art and future considerations. *Mar. Geol.* 352 (1), 111–154.
- Roca, E., 2001. The Northwest Mediterranean Basin (Valencia Trough, Gulf of Lion and Liguro-Provençal basins): structure and geodynamic evolution. *Peri-Tethyan Rift/Wrench Basins and Passive margins*, 186. In: Ziegler, P.A., Cavazza, W., Robertson, A.H.F., Crasquin-Soleau, S. (Eds.), Peri-Tethys Memoir 6, Mémoires du Muséum National d'Histoire Naturelle, Paris, pp. 671–706.
- Roca, E., Guimerà, J., 1992. The Neogene structure of the eastern Iberian margin: structural constraints on the crustal evolution of the Valencia trough (western Mediterranean). *Tectonophysics* 203, 203–218.
- Roveri, M., Flecker, R., Krijgsman, W., Lofi, J., Lugli, S., Manzi, V., Sierro, F.J., Bertini, A., Camerlenghi, A., De Lange, G., Govers, R., Hilgen, F.J., Hübscher, C., Meijer, P.T., Stoica, M., 2014. The Messinian Salinity Crisis: past and future of a great challenge for marine sciences. *Mar. Geol.* 352, 25–58.
- Séranne, M., 1999. The Gulf of Lion continental margin (NW Mediterranean) revisited by IBS: an overview. In: Durand, B., Jolivet, L., Horvath, F., Séranne, M. (Eds.), The Mediterranean Basins: Tertiary Extension within the Alpine Orogen. Volume 156. Geological Society of London, pp. 15–36 Special publication.
- Süssing, W., 2001. Tectonostratigraphy of the West Alpine Foreland; correlation of Tertiary sedimentary sequences, changes in eustatic sea-level and stress regimes. *Tectonophysics* 333, 361–400.
- Stampfli, G.M., Hööcker, C.F.W., 1989. Messinian palaeorelief from a 3D seismic survey in the Tarraco concession area (Spanish Mediterranean Sea). *Geol. Mijnb.* 68, 201–210.
- Sternai, P., Caricchi, L., Garcia-Castellanos, D., Jolivet, L., Sheldrake, T.E., Castelltort, S., 2017. Magmatic pulse driven by sea-level changes associated with the Messinian salinity crisis. *Nat. Geosci.* 10, 783–787.
- Suc, J.-P., Clauzon, G., Bessedik, M., Leroy, S., Zheng, Z., Drivaliari, A., Roiron, P., Ambert, P., Martinell, J., Doménech, R., Matias, I., Julià, R., Anglada, R., 1992. Neogene and Lower Pleistocene in Southern France and Northeastern Spain. Mediterranean environments and climate. *Cah. Micropaleontol.* 7 (1–2), 165–186.
- Suc, J.-P., Bertini, A., Combourieu-Nebout, N., Diniz, F., Leroy, S., Russo-Ermoli, E., Zheng, Z., Bessais, E., Ferrier, J., 1995. Structure of West Mediterranean vegetation and climate since 5.3 Ma. *Acta zool. Cracov.* 38 (1), 3–16.
- Suc, J.-P., Popescu, S.-M., Do Couto, D., Clauzon, G., Rubino, J.-L., Melinte-Dobrescu, M.C., Quillévéré, F., Brun, J.-P., Dumurdzanov, N., Zagorchev, I., Lesic, V., Tomic, D., Sokoutis, D., Meyer, B., Macalet, R., Rifelj, H., 2015. Marine gateway vs. fluvial stream within the Balkans from 6 to 5 Ma. *Mar. Pet. Geol.* 66, 231–245.
- Urgeles, R., Camerlenghi, A., Garcia-Castellanos, D., De Mol, B., Garcés, M., Vergés, J., Haslamk, I., Hardmank, M., 2011. New constraints on the Messinian sea level drawdown from 3D seismic data of the Ebro Margin, western Mediterranean. *Basin Res.* 23, 123–145.
- Vail, P.R., Mitchum, R.M., Todd, J.R.G., Widmier, J.M., Thompson, S., Sangree, J.B., Bubb, J.N., Hatlelid, W.G., 1977. In: Payton, C.E. (Ed.), Seismic stratigraphy and global changes of sea level: Seismic Stratigraphy – applications to Hydrocarbon Exploration. *Mem. Am. Ass. Pertol. Geol.* 26, 49–212.
- Vásquez-Urbéz, M., Arenas, C., Pardo, G., Pérez-Riváres, J., 2013. The effect of drainage reorganization and climate on the sedimentologic evolution of intermontane lake systems: the final fill stage of the Tertiary Ebro Basin (Spain). *J. Sediment. Res.* 83, 562–590.